Reactive Nitrogen, Ozone and Ozone production in the Arctic Troposphere and the Impact of Stratosphere-Troposphere Exchange

Q. Liang[1,2], J. M. Rodriguez[1], A. R. Douglass[1], J. H. Crawford[3], E. Apel[4], H. Bian[1,2], D. R. Blake[5], W. Brune[6], M. Chin[1], P. R. Colarco[1], A. da Silva[7], G. S. Diskin[3], B. N. Duncan[1], L. G. Huey[8], D. J. Knapp[4], D. D. Montzka[4], J. E. Nielsen[7,9], J. R. Olson[3], S. Pawson[7], A. J. Weinheimer[4]

[1] {NASA Goddard Space Flight Center, Atmospheric Chemistry and Dynamics Branch, Code 613.3, Greenbelt, MD 20771, USA}
[2] {Goddard Earth Sciences & Technology Center, University of Maryland, Baltimore County, Maryland, USA}
[3] {NASA Langley Research Center, Hampton,VA 23681-2199, USA}
[4] {National Center for Atmospheric Research, 1850 Table Mesa Dr., Boulder, CO 80307, USA}
[5] {University of California, 570 Rowland Hall, Irvine, CA 92697, USA}
[6] {Department of Meteorology, Pennsylvania State University, University Park, PA 16802, USA}
[7] {NASA Goddard Space Flight Center, Global Modeling and Assimilation Office, Code 610.1, Greenbelt, MD 20771, USA}
[8] {School of Earth and Atmospheric Sciences, Georgia Institute of Technology, Atlanta, GA 30332, USA}
[9] {Science Systems and Applications Inc., Lanham, Maryland, USA}

Correspondence to: Q. Liang (Qing.Liang@nasa.gov)

Abstract

We analyze the aircraft observations obtained during the Arctic Research of the Composition of the Troposphere from Aircraft and Satellite (ARCTAS) mission together with the GEOS-5 CO simulation to examine O_3 and NO_y in the Arctic and sub-Arctic region and their source attribution. Using a number of marker tracers and their probability density distributions, we distinguish various air masses from the background troposphere and examine their contribution to NO_x, O_3, and O_3 production in the Arctic troposphere. The background Arctic troposphere has mean O_3 of ~ 60 ppbv and NO_x of ~ 25 pptv throughout spring and summer with CO decreases from ~ 145 ppbv in spring to ~ 100 ppbv in summer. These observed CO, NO_x and O_3 mixing ratios are not notably different from the values measured during the 1988 ABLE-3A and the 2002 TOPSE field campaigns despite the significant changes in the past two decades in processes that could have changed the Arctic tropospheric composition. Air masses associated with stratosphere-troposphere exchange are present throughout the mid and upper troposphere during spring and summer. These air masses with mean O_3 concentration of 140-160 ppbv are the most important direct sources of O_3 in the Arctic troposphere. In addition, air of stratospheric origin is the only notable driver of net O_3 formation in the Arctic due to its sustainable high NO_x (75 pptv in spring and 110 pptv in summer) and NO_y (~800 pptv in spring and ~1100 pptv in summer) levels. The ARCTAS measurements present observational evidence suggesting significant conversion of nitrogen from HNO_3 to NO_x and then to PAN (a net formation of ~120 pptv PAN) in summer when air of stratospheric origin is mixed with tropospheric background during stratosphere-to-troposphere transport. These findings imply that an adequate representation of stratospheric O_3 and NO_y input are essential in accurately simulating O_3 and NO_x photochemistry as well as the atmospheric budget of PAN in tropospheric chemistry transport models of the Arctic. Anthropogenic and biomass burning pollution plumes observed during ARCTAS show highly elevated hydrocarbons and NO_y (mostly in the form of NO_x and PAN), but do not contribute significantly to O_3 in the Arctic troposphere except in some of the aged biomass burning plumes sampled during spring. Convection and/or lightning influences are negligible sources of O_3 in the Arctic troposphere but can have significant impacts in the upper troposphere in the continental sub-Arctic during summer.

1. Introduction

Tropospheric ozone (O_3) is important as a surface pollutant affecting air quality and is also a greenhouse gas. The Arctic has been warming at twice the global average rate over the past century (IPCC, 2007). While increases in long-lived greenhouse gases dominate Arctic warming, O_3 and other short-lived pollutants (e.g. aerosols) could also play an important role (Law and Stohl, 2007; Shindell, 2007; Quinn et al., 2007). Changes in local tropospheric O_3 affect Arctic climate by altering local radiation fluxes with maximum impact near the tropopause (Hansen et al., 1997). A recent modeling study suggested that an increase in tropospheric O_3, caused by increases in anthropogenic emissions, could have contributed about 0.3°C surface temperature increase on an annual average and about 0.4°C -0.5°C during winter and spring to the 20th-century Arctic warming (Shindell et al., 2006). The impact of possible increases in boreal forest fire emissions or changes in the stratospheric O_3 flux is not yet well quantified.

Ozone is produced locally in the Arctic troposphere from its precursors (carbon monoxide (CO), hydrocarbons, nitrogen oxides (NO_x)) emitted from anthropogenic and biomass burning sources in adjacent continents (*e.g.* Penkett and Brice, 1986; Wofsy et al., 1992; Beine et al., 1997). Additional potential sources of O_3 in the Arctic troposphere include transport of remote O_3 from the lower latitudes (Shindell et al., 2008) as well as transport from the stratosphere (Dibb et al., 2003; Allen et al., 2003). Stratospheric air contains high NO_x and nitric acid (HNO_3) and is also an important source of NO_x when injected into the Arctic troposphere (Wofsy et al., 1992; Levy et al., 1999; Law and Stohl, 2007; Liang et al., 2009). Increase in NO_x due to stratospheric intrusion is the driving mechanism that leads to enhanced O_3 production in the Arctic upper troposphere (Liang et al., 2009). A better quantification of the contribution of various anthropogenic and natural sources to O_3 in the Arctic has important implications for understanding the temporal variation and radiative impact of O_3, and how the Arctic O_3 level may change as climate warms and the stratospheric O_3 layer recovers.

The NASA Arctic Research of the Composition of the Troposphere from Aircraft and Satellite (ARCTAS) mission was conducted in April and June-July 2008 (Jacob et al., 2010). Its goal was to better understand the factors driving the changes in Arctic atmospheric composition and climate. The extensive and detailed measurements of O_3 and reactive nitrogen (NO_y) species provided an unprecedented opportunity to examine the photochemistry of O_3 and NO_x, and their sources in the Arctic. In this paper, we will use airborne observations obtained onboard the NASA DC-8 aircraft during ARCTAS and the GEOS-5 model simulated CO to examine O_3 and NO_y in the Arctic and sub-Arctic region and their source attribution. This analysis is then used to address the implications of ARCTAS measurements to our understanding of the relative contribution of different sources to O_3 and NO_y in the Arctic. Section 2 describes the observations and model used in this study. Section 3 compares the CO observations collected during ARCTAS with the model simulated CO to examine the representativeness of the ARCTAS measurements to the general characteristics of the Arctic troposphere. This helps to extrapolate the findings from the ARCTAS to achieve a better understanding of the general characteristics of the Arctic troposphere. We use a set of marker tracers to identify various air masses sampled during ARCTAS and examine their chemical composition, as described in section 4. In Sections 5 and 6, we examine NO_y, O_3, O_3 production within individual air masses sampled during ARCTAS to identify sources of O_3 in the Arctic. Conclusions are presented in Section 7.

2. Observations and Model

2.1 Observations

The NASA ARCTAS mission had two phases. The spring deployment (ARCTAS-A), based in Fairbanks Alaska, involved nine flights by the NASA DC-8 aircraft between 1 April and 21 April 2008. The summer deployment (ARCTAS-B) took place between 26 June and 14 July 2008 (nine flights) and was operated from a base in Cold Lake, Canada. Figure 1 shows the geographical distribution of flight tracks of the DC-8 aircraft during ARCTAS. Here we use measurements obtained north of 50°N. During the spring phase, the majority of the measurements are between 60°N -90°N. Measurements made during the summer phase were mainly in the sub-Arctic between 50°N -70°N.

Observations obtained onboard the DC-8 aircraft include a comprehensive suite of measurements of O_3, HO_x ($OH+HO_2$), NO_x, as well as NO_x reservoir species, hydrocarbons, halocarbons, aerosols (Jacob et al., 2010). Segregation between various air masses relies on the availability of simultaneous measurements of the marker tracers, *e.g.* CO and acetonitrile (CH_3CN) for combustion plumes and chloroflurocarbons (CFCs) for stratospheric air. A detailed list of the species used in the study and the associated instrument specifications is presented in Table 1. Multiple merge files (1-sec, 10-sec, 60-sec) were created for the ARCTAS measurements. Here, we rely on the 60-sec merge. Although many species are available at higher frequency, measurements crucial to this analysis including halocarbons and acetylene (C_2H_2) from the Whole Air Sampler – Gas Chromatography are obtained every four minutes.

2.2 GEOS-5 CO

A CO simulation was conducted for the ARCTAS period using the GEOS-5 Atmospheric Data Assimilation System (GEOS-5 ADAS) with the Modern Era Retrospective-analysis for Research and Applications (MERRA) tag (http://geos5.org/wiki/index.php?title=GEOS-5_Configuration_for_ARCTAS). Instantaneous CO is output on a 0.5° latitude by 0.67° longitude for 72 eta layers from the surface to 0.01 hPa, every 6 hours. Sources of CO include fossil fuel, biofuel, and biomass burning emissions as well as production from methane (CH_4) and non-methane hydrocarbon (NMHC) oxidation. Fossil fuel emissions are based on EDGAR 2000 with updated emissions from EPA/NEI99 for the continental USA, EMEP for Europe, BRAVE for Northern Mexico, the Zhang et al. (2009) inventory for SE Asia and China. Biofuel emissions are from Yevich et al. (2003). For biomass burning emissions, we use the Quick Fire Emission Dataset (QFED), the near-real time biomass burning emission system from the NASA Global Modeling and Assimilation Office. The QFED emissions are based on satellite retrieved fire hot spot detections from the Moderate Resolution Imaging Spectroradiometer (MODIS) fire product and scaled to yield a global emission that matches the Global Fire Emission Database (van der Werf et al., 2006). To account for production of CO from co-emitted NMHC, we apply scale factors to the direct emission sources (1.20 for fossil fuel, 1.19 for biofuel, and 1.11 for biomass burning) following Duncan et al. (2007b). We calculate CO produced from CH_4 oxidation using monthly mean CH_4 fields compiled from the long-term Global Monitoring Division (GMD) GLOBELVIEW-CH_4 observations and a yield of 1.0 of CO from CH_4 oxidation (Bian et al., 2007). Oxidation of CO is calculated using previously archived monthly OH fields from the Global Modeling Initiation (GMI) combo chemistry simulation (Duncan et al., 2007a). In addition to total CO, we also use multiple tagged tracers to track CO from anthropogenic and biomass burning pollutions emitted in different regions in the Northern Hemisphere tag (http://geos5.org/wiki/index.php?title=GEOS-5_Configuration_for_ARCTAS). We present the sum of anthropogenic pollution from North America, Europe and Asia and the sum of N. Hemispheric boreal and non-boreal biomass emissions in this study.

3. ARCTAS in the context of Arctic Spring and Summer 2008

While airborne field missions provide an extensive set of trace gas measurements over vast spatial regions, the flight plans are usually designed to target pollution plumes and thus biased towards these plumes. Thus, a simple average of these aircraft measurements may provide a biased view that is not representative of the general atmospheric composition. In this section, we i) evaluate the GEOS-5 simulated CO, and ii) examine the representativeness of the ARCTAS sampling to the general characteristics of the Arctic troposphere. Carbon monoxide is a commonly used tracer for combustion and atmospheric transport. Acetylene and CO have common combustion sources and are removed by reaction with OH in the atmosphere with different lifetime, which is about two weeks for C_2H_2 and two months for CO (e.g. Blake et al., 2003; Wofsy et al., 1992). The C_2H_2/CO ratio can be used as a tracer of pollution and it offers additional valuable information on the time since emission of pollutants and the extent of mixing with background air (*e.g.* Smyth et al, 1996; Xiao et al., 2007).

Figure 2 shows an overall comparison of the GEOS-5 simulated CO and observed CO during ARCTAS. The model results are sampled at the closest grid and time and interpolated vertically to the aircraft pressure level. Both the simulated CO and observed CO are averaged in 1-km vertical bins from the surface to 12 km. The model reproduces well the observed vertical profile (Figure 2a) and variability (r=0.69, Figure 2b) during ARCTAS-A with a systematic low bias of 15-20 ppbv in the middle and lower troposphere. The contribution from anthropogenic pollution to total CO is ~ 60% (80 ppbv) and decreases with altitude. Biomass burning emission accounts for ~ 30% (40 ppbv) of total CO and its contribution remains relatively constant throughout the troposphere. The vertical profile of CO during summer shows a distinctive peak at the surface associated with active boreal forest fires in Canada (Alvarodo et al., 2010) and a secondary peak at about 10 km due to enhanced convective outflow of anthropogenic pollution (Figure 2c), mostly from Asia (Fisher et al., 2010). The model well captures the observed vertical gradient of CO, but the simulated CO is less correlated with observations (r=0.49) and shows a more pronounced low bias (-37 ppbv) compared to spring (-25 ppbv). A significant part of the model low bias in summer is due to the inability of model to correctly represent the intensity and location of the highly localized biomass burning plumes with significantly elevated CO. The systematic low bias in the mean model CO throughout spring and summer is likely associated with too high values in the archived GMI OH fields. This low bias was previously noted in Duncan et al. (2007a) when comparing GMI simulated CO with the NOAA GMD surface observations. Although our mean tropospheric OH (0.98×10^6 molec/cm^3) and the calculated methyl chloroform (CH_3CCl_3) lifetime (6.1 y) are similar to observation-based values reported by Prinn et al. (2005) and Spivakovsky et al. (2000) (1.16×10^6 molec/cm^3 for OH concentrations, 5.7-6.0 y for CH_3CCl_3 lifetime), the lifetime of CH_3CCl_3 is heavily weighted towards the tropical lower troposphere and offers little information on the quality of the simulated OH elsewhere (Lawrence et al., 2001; Duncan et al., 2007a).

Figure 3 shows the probability density function (PDF) of CO for ARCTAS-A. The observed CO sampled by DC8 (CO_{ObsDC8}, red lines) displays a unimodal distribution in the lower and mid troposphere during spring with peaks at 160 ppbv and 145 ppbv, respectively. In the upper troposphere/lower stratosphere (UT/LS), CO_{ObsDC8} distribution is bimodal, with one peak at 125 ppbv and a secondary peak at ~ 50 ppbv representing tropospheric and stratospheric air masses, respectively. We examine the PDF of model CO along DC-8 flight track (CO_{ModDC8}, black lines). To facilitate comparison with the observed PDF, a corrected PDF of CO_{ModDC8} (black line-filled shading) is shown by adding a uniform +25 ppbv to account for the systematic low bias. The value

of +25 ppbv is determined by taking the difference between the mean CO_{ObsDC8} and the mean CO_{ModDC8} in tropospheric air mass. The corrected CO_{ModDC8} distribution agrees with the observations in the lower and mid-troposphere, and is slightly larger than observations in the UT/LS. The absence of a distinctive peak at ~ 50 ppbv in CO_{ModDC8} in the UT/LS likely implies that there are biases in stratosphere-troposphere exchange in the high latitude tropopause region in the GEOS-5 MERRA.

The PDF of CO_{ObsDC8} (red lines) during ARCTAS-B, shown in Figure 4, displays multiple peaks in the troposphere. The primary peak around 100 ppbv (90-120 ppbv) represents the background atmosphere and the two peaks between 120-160 ppbv (present in the upper and lower troposphere) and > 160 ppbv (present in the mid- and upper troposphere) are associated with fresh pollution. Acetonitrile is typically used as a tracer for biomass burning plumes (Lobert et al., 1990; Holzinger et al., 2001). The mean concentration of CH_3CN is 200 pptv for air masses with CO between 120-160 ppbv and 520 pptv for those with CO > 160 ppbv. This suggests that the measurements between 120-160 ppbv are mostly associated with anthropogenic plumes and those have CO > 160 ppbv are mostly tied to biomass burning plumes. The fact that the combustion peaks are well separated from the background suggests these are fresh pollution plumes that have not yet mixed into the background. Again to facilitate visual comparison, we add a correction of +15 ppbv to the CO_{ModDC8} which gives the best line-up between the corrected CO_{ModDC8} and CO_{ObsDC8}. Note this +15 ppbv correction is only ~40% of the summertime model mean bias (37 ppbv) as the majority of the bias is due to differences between the model and observation in a few biomass burning plumes that have very high CO levels. The corrected CO_{ModDC8} distribution (black line-filled shading) reproduces the skewness and the individual peaks in the observations. Despite the systematic bias due to OH, the fact that GEOS-5 produces the variation and distribution of the observed CO suggests that the model presents a realistic representation of the transport of pollution plumes in the Arctic troposphere as well as their mixing with the background air.

In Figures 2 and 4 we also compare CO_{ModDC8} with the simulated GEOS-5 CO in the mean atmosphere ($CO_{ModMean}$, blue shades), define as the monthly averaged CO between 50°N-90°N and 130°W-180°W, in April and July 2008 to investigate the representativeness of the ARCTAS measurements. The peak and spread of the PDF of CO_{ModDC8} (Figure 3) during April is very similar to that of $CO_{ModMean}$ in the middle and lower troposphere. Sampling in the UT/LS is biased towards the troposphere with less sampling of lower stratospheric air mass. This suggests in general the sampling during ARCTAS-A reflects well the mean composition of Arctic troposphere during spring. A similar comparison in July (Figure 4) suggests that the sampling during ARCTAS-B, on the contrary, is highly skewed towards combustion plumes at all altitudes, particularly in the lower troposphere.

We now examine the C_2H_2/CO ratio during ARCTAS as an additional marker for further examination of the age of pollution plumes and their mixing with background (Figure 5). In general, the C_2H_2/CO ratio is highly correlated with CO with r = 0.81 in spring and r = 0.69 in summer. Similar to CO (Figure 3), the PDF of the C_2H_2/CO ratio during spring displays a near-normal unimodal distribution (Figure 5a). The extended left tail is partly associated with aged stratospheric air with low C_2H_2/CO values and partly due to the reaction of C_2H_2 with bromine in the marine boundary layer during bromine explosion events (Jobson et al., 1994). Depletion of C_2H_2 has been previously observed in the Arctic in spring during many bromine explosion events (e.g. Jobson et al., 1994; Toyota et al., 2004; Ridley et al., 2007). During summer, the PDF of C_2H_2/CO ratio displays a clear bimodal distribution with one peak at ~ 0.7-0.8 pptv/ppbv corresponding to the aged background air and another peak at ~ 1.2 pptv/ppbv that is associated

with fresh anthropogenic and biomass burning pollutions (Figure 5b). The distributions of the C_2H_2/CO ratio and CO are consistent, both supporting the interpretation that the measurements obtained during ARCTAS-A are representative of a well-mixed Arctic troposphere due to slow atmospheric transport, in contrast to intensive sampling of fresh anthropogenic and biomass burning plumes that have not experienced much mixing with the background as in ARCTAS-B.

4. Air mass observed during ARCTAS

4.1 Air mass identification

We use a comprehensive set of tracers to characterize air masses sampled by the DC-8 aircraft during ARCTAS. The detailed criteria applied to define each type of air mass are listed in Table 2. Note that the thresholds of marker gases chosen to segregate air masses of different origin are highly objective and can vary significantly depending on season, location, and the question of interest. While we choose some criteria based on previous literature (O_3 > 100 ppbv for air of stratospheric origin) and the PDF distribution of CO (section 3) for combustion plumes, we heavily rely on tracer-tracer correlations for optimal segregation between different air masses (supplementary Figures 7, 8, S1 and S2). We found that the CO-NO_y, CO-CO_2 and CO-CH_4 correlations are particularly useful in determining the threshold levels of markers for distinguishing air in the stratosphere, air associated with recent STE, biomass burning and anthropogenic plumes.

We use CO and CH_3CN to distinguish anthropogenic and biomass burning pollution plumes. Since pollution plumes are not well separated from the background during spring (section 3), we use the highest quartile of CO (> 160 ppbv) to define pollution plumes. Within the pollution plumes, air masses with CH_3CN > 145 pptv are identified as biomass burning plumes and the remaining as anthropogenic pollution plumes. During summer, air masses with CO > 120 ppbv are defined as combustion plumes (Table 2). We further use CO > 160 ppbv and CH_3CN > 320 pptv to separate biomass burning air masses from anthropogenic plumes. The thresholds of CH_3CN ~ 145 pptv for ARCTAS-A and ~ 320 pptv for ARCTAS-B are chosen for optimal segregation between the biomass burning and anthropogenic pollutions based on the CO_2/CO, CH_4/CO, and C_2H_6/CO ratios (Table 2), which differ in the two type of air masses (supplementary Figures S1 and S2).

Air in the stratosphere is enriched in O_3 and depleted in surface emitted pollutants such as the long-lived CFCs (lifetime ~ 45-100 years) as well as the short-lived CO (lifetime ~ two months). Stratospheric air can enter the troposphere through rapid synoptic eddy exchange activities, *e.g.* tropopause folds, or slow global-scale diabatic descent (Holton et al., 1995). The stratosphere-to-troposphere transport time ranges between a few days during rapid tropopause folding events that intrude deeply into the troposphere to the order of a month for shallow stratosphere-troposphere-exchange (STE) intrusions followed by subsequent slow diabatic descent. The difference in transport time can lead to significantly different levels of trace gases, in particular the short-lived species such as O_3, HNO_3, Be-7 (Liang et al., 2009). We use the combination of a short-lived tracer, O_3 (> 100 ppbv), and a long-lived tracer, CFC-113 (lowest quartile, < 78 pptv) to identify air of stratospheric origin. We choose CFC-113 over the other two more common CFCs, CFC-11 and CFC-12. This is because emission of CFC-113 has significantly reduced since year 2000 (Liang et al., 2008), due to the phase-out required by Montreal protocol. Therefore low CFC-113, together with high O_3, is a better marker to distinguish air transported from the stratosphere. We apply an additional criterion, CO < 160 ppbv in spring (< 120 ppbv in summer) to exclude any samples that have mixed to some extent with fresh combustion plumes. We also use CO levels to distinguish the DC-8 sampled air that is of stratospheric-origin but has already penetrated into the troposphere through STE events (CO > 80 ppbv and 50 ppbv in spring and summer, respectively) from the air

that still resides in the lowermost stratosphere (Table 2). This is because air of stratospheric origin can have very different NO_y partitioning and photochemical properties, *e.g.* O_3 production rates, when it enters the troposphere and mixes with the tropospheric background, compared to air remains in the stratosphere. Note that the use of $O_3 > 100$ ppbv for STE air masses is a stringent criterion that distinguishes only the relatively fresh STE events from the background atmosphere.

The DC-8 aircraft also encountered a few deep convective events during ARCTAS-B. Air masses that have recently experienced deep convection contain enhanced levels of NO_x associated with freshly-ventilated air from the boundary layer and/or lightning and are depleted in HNO_3 due to scavenging (e.g. Thompson et al., 1999; Liang et al., 2007). Thus we define air as convection/lightning influenced when NO_x exceeds 200 pptv and the NO_x/HNO_3 ratio exceeds > 1.2 pptv/pptv. During ARCTAS-A, six minutes (< 0.1% of a total ~4200 minutes) of DC-8 sampled air masses contain elevated NO_x (> 100 pptv) which were of neither anthropogenic/biomass burning nor stratospheric origin. Since deep convection is not common during the high latitude spring, these measurements are most likely tied to fresh aircraft exhaustions. We therefore exclude these air samples.

The remaining air masses are defined as background. Note that the DC-8 measurements in the Arctic marine boundary layer also include a few O_3 depletion events ($O_3 < 30$ ppbv) during spring (Neuman et al., 2010) as well as local high NO_x plumes from coastal ship emissions in spring and Canadian power plants near Edmonton and Ft. McMurray in summer. We exclude these air samples in this analysis.

4.2 Air mass sampled during ARCTAS

A summary of the air mass composition sampled by the DC-8 aircraft during ARCTAS is shown in Table 3a (for ARCTAS-A) and Table 3b (for ARCTAS-B). About 58% of the spring measurements are from the background troposphere. Pollution plumes account for 21% of the observations, 17% for anthropogenic pollution and 4% for biomass burning plumes. Lowermost stratospheric air and fresh STE air account for 9% and 4% of the spring measurements, respectively. During ARCTAS-B, about 40% of the DC-8 sampled air is identified as fresh anthropogenic pollution and about 10% is attributed to fresh biomass burning plumes. However, as we discussed in section 3, the ARCTAS-B measurements are highly biased towards combustion plumes and thus the above fractionations are not representative of the general Arctic troposphere. Stratosphere air and STE together account for ~5% of the measurements. About 2% of the air sampled during ARCTAS-B was recently influenced by convection and/or lightning activities. Geographically, the majority of the convective and biomass burning plumes are located in the sub-Arctic between 50-70°N while anthropogenic and STE air masses are found throughout the Arctic and sub-Arctic (Figure 1).

The background Arctic troposphere during spring has mean CO concentration of ~145 ppbv, O_3 of ~60 ppbv, and NO_x of ~25 pptv (Table 3a). The background CO and the C_2H_2/CO ratio decrease with altitude (Figure 6ab, Table 3a), suggesting that pollution is mainly mixed into the background and trapped in the low altitudes and the atmospheric condition is stagnant. Background O_3 and NO_x remain relatively the same from spring to summer, but CO levels decrease to ~100 ppbv due to increased destruction by OH (Table 3b). Unlike spring, CO and the C_2H_2/CO ratio show little dependence on altitude, indicating efficient vertical mixing in summer. The C_2H_2/CO ratio shows a peak in the upper troposphere, a result of active ventilation of fresh pollution via deep convection.

The lowermost stratosphere, with low CO and C_2H_2/CO ratio, can reach as low as 6 km during spring, likely during low tropopause events (Figure 6ab). Significantly fewer samples of the lowermost stratospheric air (1%) were sampled during summer at > 10 km (Figure 6cd). This is

consistent with the seasonal growth of tropopause height from spring to summer. Frequent STE events have been observed throughout spring and summer. Air masses associated with fresh STE events are present at altitudes > 5 km (Figure 6). The STE air masses have higher CO and C_2H_2/CO ratio, compared to air in the lowermost stratosphere, reflecting mixing with tropospheric background air during stratosphere-to-troposphere transport.

The convective air masses observed during summer contain elevated CO (50% enhancement compared to background) and C_2H_2/CO ratio (~50%), indicating fresh ventilated surface pollution. Anthropogenic pollution plumes are present from the surface to the upper troposphere throughout spring and summer and contain elevated CO (~170 ppbv in spring and ~150 ppbv in summer) and high C_2H_2/CO ratio (~2.8 pptv/ppbv in spring and ~ 1.2 pptv/ppbv in summer). Biomass burning plumes are confined in the mid troposphere during spring with a moderate increase in CO (~220 ppbv) and C_2H_2/CO ratio (~3.2 pptv/ppbv). The majority of biomass burning air masses sampled during summer are fresh fire plumes in the lower troposphere with marked high CO (~425 ppbv) and C_2H_2/CO ratio. More detailed analysis on how anthropogenic pollution and Siberian (Spring phase) and Canadian (Summer phases) fire emissions impact atmospheric gas and aerosol composition and O_3 production can be found in Singh et al. (2010) and Alvarado et al. (2010).

5. Reactive nitrogen in the Arctic troposphere

Abundance of NO_x plays a determinative role in O_3 production in the background troposphere (Lin et al., 1988; Sillman et al., 1990; Jaeglé et al., 1998; Wennberg et al., 1998). While NO_x is present in the background atmosphere at low levels, it can be recycled between the radical forms and its long-lived reservoir species, *i.e.,* nitric acid (HNO_3) and peroxyl acetyl nitrate (PAN), which adds complexity to an accurate understanding of the NO_x budget in the atmosphere. We analyze NO_y (NO_x+PAN+ HNO_3+nitrates) and its partitioning during ARCTAS to investigate the budget and source attribution of NO_x in the Arctic and sub-Arctic troposphere. It is difficult to quantify the actual contribution of a certain source to reactive nitrogen species (same for O_3 in section 6) just based on observations. Therefore we examine the concentration of nitrogen species in individual air masses relative to those in the background. The level of elevated concentration (shown in below as Δ values relative to the background concentrations) in an individual air mass indicates its potential as a source of nitrogen species.

Reactive nitrogen in the background troposphere remains relatively constant from spring to summer (~ 300-400 pptv) (Table 3 and Figures 7 and 8). Nitrogen oxides (~ 25 pptv) on average account for 5-10% of NO_y. PAN is the largest reservoir species (~200 pptv), accounting for 50% of NO_y in spring and ~ 70% in summer. The level of HNO_3 is significantly lower than that of PAN, ~ 30 pptv in spring and ~70 pptv in summer. A small fraction of NO_y (~ 6%) is present as alkyl nitrates during summer.

The main sources of NO_y in the high latitudes troposphere are STE, anthropogenic and biomass burning emissions (Figure 7 and Table 3a). Combustion plumes are the major contributors of NO_y in the middle troposphere mainly in the form of PAN and NO_x but little HNO_3. STE events are the most significant source of NO_y above 6 km. Air masses associated with STE contain elevated levels of NO_x and HNO_3. Compared to air in the lowermost stratosphere, they contain much less NO_y (40% of that in the lowermost stratosphere) and different NO_y partitioning (less HNO_3 and more PAN). We calculate the extent of mixing between the air of stratospheric origin with the background based on the mean CO and reactive nitrogen mixing ratios in the three air masses (stratospheric air, air in the tropospheric background, and STE air) (Table 3a). We find that the change in NO_y and its partitioning from stratospheric air to STE air is mainly the result of mixing

with the background and with negligible net photochemical conversion between NO_x and its reservoirs.

All sources, including anthropogenic and biomass burning emissions, convection, and STE contribute to NO_y in the Arctic/sub-Arctic troposphere during summer (Figure 8 and Table 3b). The NO_y vs. CO relationship is more dispersed during summer, compared to a clear and compact correlation in individual air masses in spring, implying more mixing among air masses of different origin. Biomass burning air mass contains high concentrations of NO_x, PAN, and alkyl nitrates ($\Delta NO_x \sim$ 600 pptv, ΔPAN ~ 750 pptv, ΔANs ~ 200 pptv) and is the dominant contributor to NO_y ($\Delta NO_y \sim$ 1700 pptv) in the mid and lower troposphere. Anthropogenic emissions also contribute but their impacts are much less pronounced ($\Delta NO_y \sim$ 250 pptv, $\Delta NO_x \sim$ 65 pptv, ΔPAN ~ 150 pptv, and no elevated ANs and HNO_3). In the upper troposphere (> 6 km), convection, STE, and biomass burning all contribute significantly to NO_y. Convection is the dominant source of NO_x ($\Delta NO_x =$ 600 pptv) while upper tropospheric biomass burning plumes is the dominant contributor to PAN. Air masses associated with STE contains high NO_y comparable to that in convective air mass. The STE air mass displays high NO_x ($\Delta NO_x \sim$ 100 pptv) and HNO_3 ($\Delta HNO_3 \sim$ 400 pptv) as stratospheric air is commonly enriched with NO_x and HNO_3.

The STE air is also significantly elevated in PAN (50% more than the background), with mean concentration (~ 320 pptv) almost comparable to that in anthropogenic plumes (~ 355 pptv). The main sources of PAN in the atmosphere are biomass burning and anthropogenic emissions. Oxidation of non-methane hydrocarbons (NMHC) within combustion plumes can rapidly convert NO_x to form PAN (*e.g.* Aikin et al., 1983; Singh et al., 1992; Alvarado et al., 2010). Our definition of STE air masses (CO < 160 ppbv for spring and CO < 120 ppbv for summer) excludes the possibility of mixing with fresh combustion plumes which could have contributed to elevated PAN. Further calculation based on mean concentrations of CO and nitrogen species (Table 3b) suggests that mixing with tropospheric background air can increase PAN to ~ 200 pptv in the STE air mass (from 70 pptv in lowermost stratospheric air). The remaining ~ 120 pptv increase in PAN can only be explained by active photochemical production. As air from the stratosphere, which contains high NO_x and HNO_3, mixes with the tropospheric background, it provides a direct source of NO_x as well as an indirect source through releasing NO_x via HNO_3 destruction. The resulted NO_x can react with acetyl radicals from the breakdown of acetaldehyde to form PAN. While many NMHC have lifetimes too short to exert a significant impact on PAN production in the background troposphere, ethane (C_2H_6), which has a mean atmospheric lifetime of ~ 2 months and up to 10 months in winter (Rudolph et al., 1995; Xiao et al., 2008), is the most likely source of acetaldehyde and has been demonstrated to contribute to PAN formation in the UT/LS (Aikin et al., 1983). Our earlier modeling study, Liang et al. (2009), conducted a detailed budget analysis of NO_y in the Arctic using the GMI CTM which contains a fully-coupled tropospheric and stratospheric chemistry scheme. The calculated result suggests that significant conversion of nitrogen from HNO_3 to NO_x and then to PAN within STE air masses in the upper Arctic troposphere during summer. The ARCTAS measurements are in accordance with our theoretical modeling analysis and present the first observation evidence of mixing of stratospheric air with free tropospheric background air as a significant source of PAN in the upper troposphere. This chemical mechanism may likely explain the current difficulty in several tropospheric chemistry transport models (CTMs), in reproducing the observed PAN during ARCTAS (Singh et al., 2010; Alvarado et al., 2010). Unlike GMI, these tropospheric CTMs do not have a well specified stratospheric input of NO_y, therefore an inadequate representation of PAN production in the Arctic upper troposphere.

6. Ozone and ozone production in the Arctic troposphere

The photochemical balance between O_3 production and loss is an intricate play between NO_x, HO_x, and O_3 (Jaeglé et al., 1998; Wennberg et al., 1998). In this section, we examine O_3, O_3 production rate and its dependence on NO_x and HO_x to understand the sources of O_3 in the Arctic and sub-Arctic troposphere.

Ozone is produced in the troposphere mainly through the following chemical reactions,

$$OH + CO \xrightarrow{O_2} HO_2 + CO_2 \quad (1)$$
$$HO_2 + NO \rightarrow OH + NO_2 \quad (2)$$
$$NO_2 + hv \rightarrow NO + O \quad (3)$$
$$O + O_2 \rightarrow O_3 \quad (4)$$

Net: $CO + 2O_2 \rightarrow CO_2 + O_3$

with reaction (2) being the rate-limiting step. Ozone can also be produced from reaction of peroxy radicals (RO_2) with NO:

$$RO_2 + NO \rightarrow CH_2O + HO_2 + NO_2 \quad (5)$$

Ozone is destroyed in the troposphere through photolysis and reaction with HO_x ($OH + HO_2$):

$$O_3 + hv \rightarrow O(^1D) + O_2$$
$$O(^1D) + H_2O \rightarrow 2OH \quad (6)$$
$$HO_2 + O_3 \rightarrow OH + 2O_2 \quad (7)$$
$$OH + O_3 \rightarrow HO_2 + O_2 \quad (8)$$

We use the O_3 product and loss rates calculated by the NASA Langley box model (Olson et al., 2004) constrained by chemical and physical parameters measured by the DC-8 aircraft. For this study, we use mostly the instantaneous product and loss rates. Note catalytic destruction of O_3 by bromine radicals is also included in the Langley box model to account for the O_3 depletion events sampled during ARCTAS. For simplicity and clarity, we exclude data that contain elevated bromine (BrO > 1.5 pptv). The calculated net O_3 production (formation-destruction) rates, $NP(O_3)$, can be approximated as:

$$NP(O_3) = P(O_3) - L(O_3)$$
$$= K_2[HO_2][NO] + K_5[RO_2][NO] - K_6[H_2O][O(^1D)] - K_7[HO_2][O_3] - K_8[OH][O_3]$$

Figure 9 shows the dependence of the calculated instantaneous $NP(O_3)$ on levels of NO_x during ARCTAS for high and low HO_x conditions and vice versa. While NO_x concentration remains relatively unchanged from spring to summer, O_3 production rate during summer is ~10 times higher than that calculated for spring, due to active photochemistry with increasing insolation. The level of NO_x plays a determinative role in the photochemical production of O_3. The $NP(O_3)$ increases rapidly with increasing levels of NO_x, suggesting that the Arctic troposphere is in the NO_x-limited regime. The rate $NP(O_3)$ increases with increasing NO_x is dependent on the abundance of HO_x radicals. When HO_x is high (> 4 pptv in spring and > 10 pptv in summer which occur mostly in combustion plumes), the $NP(O_3)$ increases drastically as NO_x increases. At low HO_x concentrations (background and air of stratospheric origin), the $NP(O_3)$ displays a weak increase with increasing NO_x as both production (reaction 2) and loss (reactions 7 and 8) are slow. The dependence of $NP(O_3)$ on HO_x is rather complex, impacted by levels of NO_x. On the one hand, HO_x can enhance O_3 production through reaction (2). On the other hand, it provides a reaction partner for O_3 destruction in reactions (7) and (8). At high NO_x levels (*e.g.* fresh combustion plumes, STE events, and convection), the $NP(O_3)$ show a positive dependence on HO_x concentrations and increases as HO_x increases. When NO_x is low (< 40 pptv, *i.e.* background and air of stratospheric origin), the

$NP(O_3)$ is either insensitive to HO_x (spring) or decreases with increasing HO_x and becomes negative when HO_x exceeds 20 pptv (summer).

The mean background O_3 in the Arctic and sub-Arctic troposphere remain relatively constant from spring to summer, increasing from 30-40 ppbv at the surface to 60-70 ppbv in the middle and upper troposphere (Figure 10be and Table 3). The middle troposphere (3-8 km) shows net O_3 destruction while the lower (< 3 km) and upper troposphere (> 8 km) has $NP(O_3)$ greater than zero (net O_3 formation), regulated by the mean NO_x concentration. $NO_x \sim 20$ pptv is a critical level (Klonecki and Levy, 1997) in the Arctic troposphere that separates the middle troposphere ($NO_x <$ 20 pptv, net O_3 destruction regime, Figure 10cf) from the lower and upper troposphere where NO_x exceeds 20 pptv, hence, net O_3 production (Figure 10cf).

STE events are the most significant source of O_3 in the Arctic during spring and summer, particularly in the upper troposphere (Figure 10). Air mass associated with recent STE intrusions has mean O_3 mixing ratio of ~150 ppbv (vs. ~70 ppbv in background air between 6-12 km). The STE air mass also shows net O_3 formation with instantaneous $NP(O_3)$ as high as ~ 2 ppbv/day in spring and ~ 5 ppbv/day in summer. The change from near zero $NP(O_3)$ in the lowermost stratospheric air to positive values is mainly the result of increasing HO_x. Air of stratospheric origin contains high NO_x and its O_3 production rate is highly dependent on the level of HO_x, as discussed above. As stratospheric air entrains into the troposphere during STE, it mixes with the surrounding background air that has higher water vapor, therefore increases the production of HO_x and HO_x concentration. This results in an increase in $NP(O_3)$ from near zero to net O_3 formation.

Convection/lightning is an important source of O_3 during ARCTAS-B. The summertime convective/lightning air mass is elevated in O_3 ($\Delta O_3 \sim 10$ ppbv, Table 3b) and displays high net O_3 production. The springtime biomass burning air mass shows active O_3 production (mean instantaneous $NP(O_3) \sim 2$ ppbv/day and $\Delta O_3/\Delta CO = 0.22$) and an average of 16 ppbv increase in O_3. In contrast, the biomass burning air masses sampled in summer, although showing very high positive $NP(O_3)$ values, display no elevated O_3. Alvarado et al. (2010) conducted a detailed analysis of NO_x and PAN photochemistry in boreal fire plumes during ARCTAS-B and their impact on O_3 and found little evidence of O_3 formation in the smoke plumes in either the aircraft, satellite, or model results, in accordance with our findings. Paris et al. (2010) also found negative O_3/CO ratio (-0.04 ppbv/ppbv), indicating photochemical destruction of O_3 in the summertime Siberian fire plumes observed during the YAK-AEROSIB/POLARCAT experiment. The seasonal difference in O_3 formation within the biomass burning plumes is likely due to differences in the O_3 production efficiency, defined as the number of O_3 molecules produced per molecule of NO_x consumed (Jacob 1999). While the $NP(O_3)$ in the summer fire plumes are high, this high production is not sustainable as O_3 production efficiency is low and NO_x are rapidly converted to PAN in ~2 hours (Alvarado et al., 2010). The anthropogenic air mass in general contains significantly less NO_x than the other two tropospheric air masses (biomass burning, convection) (Figures 7 and 8) and therefore weaker O_3 production (Figure 10). Despite the positive $NP(O_3)$ rates, the anthropogenic air mass sampled during both ARCTAS-A and ARCTAS-B show no elevated O_3, compared to the background, throughout most of the troposphere.

As we have discussed in section 2.1, measurements obtained during ARCTAS-B are concentrated in the sub-Arctic between 50°N-70°N. The derived conclusions may not represent the true Arctic troposphere as more convection occurs in the continental sub-Arctic and it is closer to pollution sources. We narrow our investigation to focus only on the measurements obtained north of 70°N during ARCTAS-B (Figure 11). While there is significant fraction of convection/lightning air masses identified during ARCTAS-B, none is sampled in the deep Arctic. Air mass associated

with STE events is the only notable contributor to NO_x and O_3 north of 70°N. In addition, the STE air mass is the only air mass that displays net O_3 formation above 2 km. The mean 24-hour averaged $NP(O_3)$ (calculated by the Langley box model) in the fresh STE air mass sampled during ARCTAS-B is ~0.9 ppbv/day. These findings confirm our previous proposition that STE, in addition to its direct contribution to O_3, is the driving mechanism of net O_3 formation in the Arctic upper troposphere as calculated in the GMI Combo CTM (0-10 ppbv/month in July) (Liang et al., 2009).

7. Conclusions

The NASA ARCTAS mission presents a unique opportunity and an extensive suite of measurements to examine O_3 photochemistry in the Arctic troposphere. A close look at the observations of CO and the C_2H_2/CO ratio suggests that the DC-8 aircraft measurements obtained during spring (ARCTAS-A) are representative of the mean Arctic troposphere. Measurements obtained during the summer deployment (ARCTAS-B) are highly biased towards pollution plumes, a fact to consider in understanding the mean chemical composition of the summertime Arctic troposphere and the impact of pollution plumes.

We conducted a detailed analysis using aircraft observations obtained during ARCTAS to examine O_3 and NO_y in the Arctic and sub-Arctic region and their source attribution. Using a number of marker tracers, we were able to identify various air masses from the background, including anthropogenic pollution, biomass burning emissions, air masses associated fresh stratosphere-troposphere exchange, and convection and/or lightning influences.

The background Arctic troposphere has mean O_3 of ~ 60 ppbv and NO_x of ~ 25 pptv throughout spring and summer. Mean CO mixing ratio decreases from ~ 145 ppbv during spring to ~ 100 ppbv in summer. The Arctic troposphere is in the NO_x-limited regime with much of the free troposphere shows net O_3 destruction due to its low NO_x concentration. Extensive aircraft sampling of the Arctic troposphere were available from the earlier Tropospheric O_3 Production about the Spring Equinox (TOPSE) campaign in spring 2002 (Atlas et al., 2003) and the Arctic Boundary Layer Expedition (ABLE 3A) during summer 1988 (Harriss et al., 1992). Measurements from these previous missions show a springtime mean CO ~ 154 ppbv, O_3 ~ 67 ppbv, and NO_x ~ 17 pptv (TOPSE) (Stroud et al., 2003) and a summertime mean CO ~ 100 ppbv, O_3 ~ 70 ppbv, and NO_x ~ 10-50 pptv (ABLE 3A) (Jacob et al., 1992) at 3-6 km in the Arctic mid-troposphere. Consider the likely variations associated with differences in air mass sampling and interannual variability, the ARCTAS measurements indicate that these important tropospheric trace gases, CO, NO_x and O_3, have remain relatively unchanged in the Arctic mid-troposphere in the past two decades, despite the significant changes in processes that could have had a notable impact on the Arctic atmospheric composition, *e.g.* emissions regulation in European and N. American, rapid industrialization of East Asia, destruction of the stratospheric O_3 layer.

Air masses associated with recent stratosphere-troposphere exchange are present at > 5 km during spring and summer. These air masses with mean O_3 concentration of 140-160 ppbv are the most important direct sources of O_3 in the Arctic (> 70°N) troposphere. Air of stratospheric origin is also significantly elevated in NO_x (mean ~ 75 pptv in spring and 110 pptv in summer) and HNO_3 (mean ~ 290 pptv in spring and 500 pptv in summer) which will further release NO_x through photochemical destruction. Driven by the high levels of NO_x, these air masses display active net O_3 formation with instantaneous production rates as high as ~ 2 ppbv/day in spring and ~ 5 ppbv/day in summer and is the main driver of net O_3 production in the Arctic free troposphere. The ARCTAS measurements also present observational evidence suggesting significant conversion of nitrogen

from HNO_3 to NO_x and then to PAN within STE air masses during summer (a net formation of ~120 pptv PAN), in accordance with our previous modeling analysis (Liang et al., 2009). This implies that the impact of NO_y-enriched stratospheric air on tropospheric NO_x, and therefore O_3 production, can be extended much further as the resulted PAN is transported to the lower altitudes and releases NO_x downwind through thermal decomposition (e.g. Moxim et al., 1996, Honrath et al., 1996). Although the ARCTAS measurements present clear evidence of stratosphere-troposphere exchange as a significant source of reactive nitrogen in the Arctic troposphere, a quantitative estimate of the impact of the influx of NO_y from the stratosphere on the troposphere NO_x, PAN, and subsequently O_3 production is yet to be determined through more comprehensive modeling studies.

Although anthropogenic and biomass burning pollution plumes show highly elevated hydrocarbons and NO_y (mostly in the form of NO_x and PAN), there is little evidence that these pollution plumes contribute significantly to O_3 in the Arctic troposphere, except the aged Siberia biomass burning plumes during Spring. However, it is important to point out that anthropogenic and biomass burning emissions can still exert an impact on O_3 in the Arctic through increasing the background O_3 in the mid-latitudes which then enters the polar troposphere through long-range transport, as demonstrated by Shindell et al. (2008). Convection and/or lightning influences are of negligible importance as a source of O_3 in the Arctic but can have significant impacts in the upper troposphere in the continental sub-Arctic during summer.

Acknowledgements. The authors thank R. C. Cohen for providing nitrates measurements. This research was supported by the NASA ARCTAS and MAP programs.

References.

Aikin, A.C., Herman, J. R., Maier, E. J. R., and McQuillan, C. J.: Influence of Peroxyacetyl nitrate (PAN) on odd nitrogen in the troposphere and lower stratosphere, Planetary and Space Science, 31, 1075-1082, 1983.

Allen, D. J., Dibb, J. E., Ridley, B., Pickering, K. E., and Talbot, R.W.: An estimate of the stratospheric contribution to springtime tropospheric ozone maxima using TOPSE measurements and beryllium-7 simulations, J. Geophys. Res., 108(D4), 8355, doi:10.1029/2001JD001428, 2003.

Alvarado, M. J., Logan, J. A., Mao, J., et al.: Nitrogen oxides and PAN in plumes from boreal fires during ARCTAS-B and their impact on ozone: an integrated analysis of aircraft and satellite observations, Atmos. Chem. Phys., 10, 9739-9760, doi:10.5194/acp-10-9739-2010, 2010.

Apel, E. C, Hills, A. J., Lueb, R., Zindel, S., Eisele, S., and Riemer, D. D.: A fast-GC/MS system to measure C-2 to C-4 carbonyls and methanol aboard aircraft, J. Geophys. Res., 108, 8794, doi:10.1029/2002JD003199, 2003.

Atlas, E. L., Ridley, B. A., and Cantrell, C. A.: The Tropospheric Ozone Production about the Spring Equinox (TOPSE) Experiment: Introduction, J. Geophys. Res., 108(D4), 8353, doi:10.1029/2002JD003172, 2003.

Beine, H. J., Jaffe, D. A., Herring, J. A., Kelley, J. A., Krognes, T., and Stordal, F.: High-Latitude Springtime Photochemistry. Part I: NOx, PAN and Ozone Relationships, Journal of Atmospheric Chemistry, 27, 127-153, 1997.

Bian, H., Chin, M., Kawa, S. R., Duncan, B., Arellano, A., and Kasibhatla, P.: Sensitivity of global CO simulations to uncertainties in biomass burning sources, J. Geophys. Res., 112, D23308, doi:10.1029/2006JD008376, 2007.

Blake, N. J., Blake, D. R., Simpson, I. J., et al: NMHCs and halocarbons in Asian continental outflow during the Transport and Chemical Evolution over the Pacific (TRACE-P) field campaign: comparison with PEM-West B, J. Geophys. Res., 108, 8806, doi:10.1029/2002JD003367, 2003.

Brune, W. H., Tan, D., Faloona, I. F., et al.: OH and HO_2 chemistry in the North Atlantic free troposphere, Geophys. Res. Lett., 26, 3077–3080, 1999.

Cleary, P. A., Wooldridge, P. J., and Cohen, R. C.: Laser-induced fluorescence detection of atmospheric NO2 using a commercial diode laser and a supersonic expansion, Appl. Opt., 41, 6950–6956, 2002.

Dibb, J. E., Talbot, R. W., Scheuer, E., Seid, G., DeBell, L., Lefer, B., and Ridley, B.: Stratospheric influence on the northern North American free troposphere during TOPSE: 7Be as a stratospheric tracer, J. Geophys. Res., 108(D4), 8363, doi:10.1029/2001JD001347, 2003.

Diskin, G. S., Podolske, J. R., Sachse, G. W., and Slate, T. A.: Open-Path Airborne Tunable Diode Laser Hygrometer, in Diode Lasers and Applications in Atmospheric Sensing, SPIE Proceedings 4817, edited by: Fried, A., 196–204, 2002.

Duncan, B. N., Strahan, S. E., Yoshida, Y., Steenrod, S. D., and Livesey, N.: Model study of the cross-tropopause transport of biomass burning pollution, Atmos. Chem. Phys., 7, 3713-3736, 2007a.

Duncan, B. N., Logan, J. A., Bey, I., Megretskaia, I. A., Yantosca, R. M., Novelli, P. C., Jones, N. B., and Rinsland, C. P.: The global budget of CO, 1988-1997: source estimates and validation with a global model, J. Geophys. Res., 112, D22301, doi:10.1029/2007JD008459, 2007b.

Fisher, J. A., Jacob, D. J., Purdy, M. T., Kopacz, M., Le Sager, P., Carouge, C., Holmes, C. D., Yantosca, R. M., Batchelor, R. L., Strong, K., Diskin, G. S., Fuelberg, H. E., Holloway, J. S., Hyer, E. J., McMillan, W. W., Warner, J., Streets, D. G., Zhang, Q., Wang, Y., and Wu, S.: Source attribution and interannual variability of Arctic pollution in spring constrained by aircraft (ARCTAS, ARCPAC) and satellite (AIRS) observations of carbon monoxide, Atmos. Chem. Phys., 10, 977–996, doi:10.5194/acp-10-977-2010, 2010.

Hansen, J., Sato, M., Ruedy, R.: Radiative forcing and climate response, J. Geophys. Res., 102, D6, 683106864, 1997.

Harriss, R. C., Wofsy, S. C., Bartlett, D. S., et al.: The Arctic Boundary Layer Expedition (ABLE-3A): July-August 1988, J. Geophys. Res., 97, 16,383-16,394, 1992.

Holton, J. R., Haynes, P. H., McIntyre, M. E., Douglass, A. R., Rood, R. B., and Pfister, L.: Stratosphere-troposphere exchange, Rev. Geophys., 33, 403-439, 1995.

Holzinger, R., A. Jordan, A. Hansel, and W. Lindinger, Automobile emissions of acetonitrile: Assessments of its contribution to the global source, Atmos. Environ., 38, 187– 193, 2001.

Honrath, R.E., Hamlin, A.J., Merrill, J.T.: Transport of ozone precursors from the Arctic troposphere to the North Atlantic region. J. Geophys. Res., 101, 29335-29351, 1996.

IPCC Fourth Assessment Report, Climate Change 2007, IPCC, Geneva, Switzerland.

Jacob, D. J., *Introduction to Atmospheric Chemistry*, Princeton University Press, page 240, 1999.

Jacob, D.J., Crawford, J.H., Maring, H., et al.: The ARCTAS aircraft mission: design and execution, Atmos. Chem. Phys. 10, 5191-5212, 2010.

Jacob, D.J., Wofsy, S.C., Bakwin, P.S., et al.: Summertime photochemistry at high northern latitudes. J. Geophys. Res. 97 (D15), 16421-16431, 1992.

Jaeglé, L., Jacob, D. J., Brune, W. H., Tan, D., Faloona, I. C., Weinheimer, A. J., Ridley, B. A., Campos, T. L., and Sachse, G. W.: Sources of HO_x and production of ozone in the upper troposphere over the United States, Geophys. Res. Lett., 25(10), 1709-1712, 1998.

Jobson, B.T., Niki, H., Yokouchi, Y., Bottenheim, J., Hopper, F., Leaitch, R.: Measurements of C2–C6 hydrocarbons during the 1992 Polar Sunrise Experiment: Evidence of Cl-atom and Br-atom chemistry, J. Geophys. Res. 99, 25355–25368, 1994.

Klonecki, A. A., and Hevy, H., II: Tropospheric chemical ozone tendencies in the CO-CH_4-NO_y-H_2O system: Their sensitivity to variations in environmental parameters and their application to a GCTM study, J. Geophys. Res., 102, 21,221-21,237, 1997.

Law, K. S., and A. Stohl: Arctic Air Pollution: Origins and Impacts, Science, 315, 1537, doi:10.1126/science.1137695, 2007.

Lawrence, M. G., Jockel, P, von Kuhlmann, R.: What does the global mean OH concentration tell us? Atmos. Chem. Phys., 1, 37-49, 2001.

Levy, H., II, Moxim, W. J., Klonecki, A. A., and Kasibhatla, P. S.: Simulated tropospheric NOx: Its evaluation, global distribution and individual source contributions, J. Geophys. Res., 104, 26,279-26,306, 1999.

Liang, Q., Jaeglé, L., Hudman, R. C., et al.: Summertime influence of Asian pollution in the free troposphere over North America, J. Geophys. Res., 112, D12S11, doi:10.1029/2006JD007919, 2007.

Liang, Q., Stolarski, R. S., Douglass, A. R., Newman, P. A., and Nielsen, J. E.: Evaluation of emissions and transport of CFCs using surface observations and their seasonal cycles and the GEOS CCM simulation with emissions-based forcing, J. Geophys. Res., 113, D14302, doi:10.1029/2007JD009617, 2008.

Liang, Q., Douglass, A. R., Duncan, B. N., Stolarski, R. S., and Witte, J. C.: The governing processes and timescales of stratosphere-to-troposphere transport and its contribution to ozone in the Arctic troposphere, Atmos. Chem. Phys., 9, 3011-3025, 2009.

Lin, X., Trainer, M., and Liu, S. C.: On the nonlinearity of the tropospheric ozone production, J. Geophys. Res., 93, 15,879-15,888, 1988.

Lobert, J. M., D. H. Scharffe, W. M. Hao, and P. J. Crutzen, Importance of biomass burning in the atmospheric budgets of nitrogen-containing gases, Nature, 346, 552– 554, 1990.

Moxim, W.J., Levy, H., Kasibhalta, P.S.: Simulated global tropopsheric PAN: its transport and impact on NO_x, J. Geophys. Res., 101, 12621-12638, 1996.

Neuman, J. A., Nowak, J. B., Huey, L. G., Burkholder, J. B., Dibb, J. E., Holloway, J. S., Liao, J., Peischl, J., Roberts, J. M., Ryerson, T. B., Scheuer, E., Stark, H., Stickel, R. E., Tanner, D. J., and Weinheimer, A.: Bromine measurements in ozone depleted air over the Arctic Ocean, Atmos. Chem. Phys., 10, 6503-6514, doi:10.5194/acp-10-6503-2010, 2010.

Olson, J. R., Crawford, J. H., Chen, G. et al.: Testing fast photochemical theory during TRACE-P based on measurements of OH, HO_2, and CH_2O, J. Geophys. Res., 109, D15S10, doi:10.1029/2003JD004278, 2004.

Paris, J.-D., Stohl, A., Nédélec, P. , Arshinov, M. Yu. , Panchenko, M. V., Shmargunov, V. P., Law, K. S., Belan, B. D., and Ciais, P.: Wildfire smoke in the Siberian Arctic in summer: source characterization and plume evolution from airborne measurements, Atmos. Chem. Phys., 9, 9315-9327, 2009.

Penkett, S. A., and Brice, K. A.: The spring maximum in photooxidants in northern-hemisphere troposphere, Nature, 319, 655-657, 1986.

Prinn, R. G., Huang, J., Weiss, R. F., et al.: Evidence for variability of atmospheric hydroxyl radicals over the past quarter century, Geophys. Res. Lett., 32, L07809, doi:10.1029/2004GL022228, 2005.

Quinn, P. K., Bates, T. S., Baum, E., Doubleday, N., Fiore, A. M., Flanner, M., Fridlind, A., Garrett, T. J., Koch, D., Menon, S., Shindell, D., Stohl, A., and Warren, S. G.: Short-lived pollutants in the arctic: Their climate impact and possible mitigation strategies, Atmos. Chem. Phys., 8, 1723–1735, 2007.

Ridley, B. A., Zeng, T., Atlas, E. L., Browell, E. V., Hess, P. G., Orlando, J. J., Chance, K., and Richter, A.: An ozone depletion event in the sub-arctic surface layer over Hudson Bay, Canada, J. Atmos. Chem., Vol 57, 3, 255-280, doi:10.1007/s10874-007-9072, 2007.

Rudolph, J.: The tropospheric distribution and budget of ethane, J. Geophys. Res., 100(D6), 11,369– 11,381, 1995.

Singh, H. B., O'Hara, D., Herlth, D., Bradshaw, J. D., Sandholm, S. T., Gregory, G. L., Sachse, G. W., Blake, D. R., Crutzen, P. J., and Kanakidou, M. A.: Atmospheric measurements of peroxyacetyl nitrate and other organic nitrates at high latitudes: Possible sources and sinks. *J. Geophys. Res., 97*(D15), 16511-16522, doi:10.1029/91JD00889, 1992.

Singh, H. B., Anderson, B. E., Brune W. H., et al.: Pollution influences on atmospheric composition and chemistry at high northern latitudes: Boreal and California forest fire emissions, Atmos. Environ., 44, 4553-4564, 2010.

Shindell, D.: Local and remote contributions to Arctic warming, Geophys. Res. Lett, 34, L14704, doi: 10.1029/2007GL030221, 2007.

Shindell, D., Faluvegi, F., Lacis, A., Hansen, J., Ruedy, R., and Aguilar, E.: Role of tropospheric ozone increases in 20th-century climate change, J. Geophys. Res., 111, D08302, doi:10.1029/2005JD006348, 2006.

Shindell, D. T., Chin, M., Dentener, F.: A multi-model assessment of pollution transport to the Arctic, Atmos. Chem. Phys., 8, 5353-5372, 2008.

Sillman, S., Logan, J. A., and Wofsy, S. C.: The sensitivity of ozone to nitrogen oxides and hydrocarbons in regional ozone episodes, J. Geophys. Res., 95, 1837-1852, 1990.

Slusher, D. L., Huey, L. G., Tanner, D. J., Flocke, F. M., and Roberts, J. M.: A thermal dissociation-chemical ionization mass spectrometry (TD-CIMS) technique for the simultaneous measurement of peroxyacyl nitrates and dinitrogen pentoxide, J. Geophys. Res., 109, D19315, doi:10.1029/2004JD004670, 2004.

Smyth, S., Bradshaw, J., Sandholm, S., et al.: Comparison of free tropospheric western Pacific air mass classification schemes for the PEM-West A experiment, J. Geophys. Res., 101(D1), 1743–1762, 1996.

Spivakovsky, C. M., Logan, J. A., Montzka, S. A., et al.: Three-dimensional climatological distribution of tropospheric OH: Update and evaluation, J. Geophys. Res., 105(D7), 8931–8980, 2000.

Stroud, C., Madronich, S., Atlas, E., et al.: Photochemistry in the arctic free troposphere: NOx budget and the role of odd nitrogen reservoir recycling, Atmos. Environ., 37, 3351-3364, 2003.

Thompson, A. MM., Sparling, L. C., Kondo, Y., Anderson, B. E., Gregory, G. L., and Sachse, G. W.: Perspectives on NO, NOy, and fine aerosol sources and variability during SONEX, Geophys. Res. Lett., 26, 3073-3076, 1999.

Toyota, K., Kanaya, Y., Takahashi, M., and Akimoto, H.: A box model study on photochemical interactions between VOCs and reactive halogen species in the marine boundary layer, Atmos. Chem. Phys., 4, 1961-1987, 2004.

van der Werf, G. R., Randerson, J. T., Giglio, L., Collatz, G. J., Kasibhatla, P. S., Arellano, A. F.: Interannual variability in global biomass burning emissions from 1997 to 2004, Atmos. Chem. Phys., 6, 3423-3441, 2006.

Weinheimer, A. J., Walega, J. G., Ridley, B. A., Gary, B. L., Blake, D. R., Blake, N. J., Rowland, F. S., Sachse, G. W., Anderson, B. E., and Collins, J. E.: Meridional distributions of NOx, NOy, and other species in the lower stratosphere and upper troposphere during AASE II, Geophys. Res. Lett., 21, 2583–2586, 1994.

Wennberg, P. O., Hanisco, T. F., Jaeglé, L., et al.: Hydrogen Radicals, Nitrogen Radicals, and the Production of O_3 in the Upper Troposphere, Science, 279, 49-53, 1998.

Wofsy, S. C., Sachse, G. W., Gregory, G. L., et al.: Atmospheric chemistry in the Arctic and sub-Arctic: Influence of natural fires, industrial emissions, and stratospheric inputs, J. Geophys. Res., 97(D15), 16,731–16,746, 1992.

Xiao, Y., Jacob, D. J., and Turquety, S.: Atmospheric acetylene and its relationship with CO as an indicator of air mass age, J. Geophys. Res., 112, D12305, doi:10.1029/2006JD008268, 2007.

Xiao, Y. P., Logan, J. A., Jacob, D. J., Hudman, R. C., Yantosca, R., and Blake, D. R.:The global budget of ethane and regional constraints on U.S. sources, J. Geophys. Res., doi:10.1029/2007JD009415, 2008.

Yevich, R. and Logan, J. A.: An assessment of biofuel use and burning of agricultural waste in the developing world, Global Biogeochem. Cycles, 17(4), 1095, doi:10.1029/2002GB001952, 2003.

Zhang, Q., Streets, D. G., Carmichael, G. R., He, K. B., Huo, H., Kannari, A., Klimont, Z., Park, I. S., Reddy, S., Fu, J. S., Chen, D., Duan, L., Lei, Y., Wang, L. T., and Yao, Z. L.: Asian emissions in 2006 for the NASA INTEX-B mission, Atmos. Chem. Phys., 9, 5131–5153, 2009.

Table 1. Summary of ARCTAS observations used in this study.

Species	Instrument & Methods	Reference
CO	Tunable Diode Laser Absorption Spectroscopy (TDLAS)	*Diskin et al.* (2002)
O_3, NO, NO_2, NO_y *	Chemiluminescence	Weinheimer et al. (1994)
PAN	Chemical Ionization Mass Spectrometry (CIMS)	Slusher et al. (2004)
Alkyl nitrates	Thermal-Dissociation Laser Induced Fluorescence (TD-LIF)	Cleary et al. (2002)
OH, HO_2 *	Laser Induced Fluorescence (LIF)	Brune et al. (1999)
CH_3CN *	Gas Chromatography – Mass Spectrometry (GC-MS)	Apel et al. (2003)
CFC-113, C_2H_2	Whole Air Sampler – Gas Chromatography (WAS-GC)	Blake et al. (2003)

*Multiple sets of measurements were available for several species used in this study, *i.e.* NO_2, OH, HO_2, HNO_3, CH_3CN. The different measurements broadly agree with each other and the choice of measurements does not affect the conclusion of this study.

Table 2. Air mass characterization criteria.

Air mass type	Criteria	
	ARCTAS-A	ARCTAS-B
Stratospheric air	O_3 > 100 ppbv; CFC-113 < 78 [a] pptv; CO < 80 [b] ppbv	O_3 > 100 ppbv; CFC-113 < 78 [a] pptv; CO < 50 [b] ppbv
Stratosphere-troposphere exchange	O_3 > 100 ppbv; CFC-113 < 78 [a] pptv; 80 [b] ppbv ≤ CO < 160 ppbv	O_3 > 100 ppbv; CFC-113 < 78 [a] pptv; 50 [b] ppbv ≤ CO < 120 ppbv
Biomass burning	CO >160 [c] ppbv; CH_3CN >145 [d] pptv	CO >120 [c] ppbv; CH_3CN >320 [d] pptv
Anthropogenic	CO >160 [c] ppbv; CH_3CN ≤145 [d] pptv	CO >120 [c] ppbv; CH_3CN ≤320 [d] pptv
Convection/Lightning	NO_x > 100 pptv; NO_x/HNO_3 > 1.2 pptv/pptv	NO_x > 200 pptv; NO_x/HNO_3 > 1.2 pptv/pptv

[a] The 78 pptv threshold is the 25 percentile value for CFC-113.
[b] The CO ~ 80 ppbv threshold level between stratospheric air and air associated with stratosphere-troposphere exchange are determined based on scattering plots of CFC-113, CH_3CN, SO_2 vs. CO during ARCTAS-A. The CO ~ 50 ppbv threshold for ARCTAS-B is determined based on the scattering plots of CH_4, CO_2, NO_y vs. CO.
[c] The CO ~ 160 ppbv threshold level during ARCTAS-A for biomass burning and anthropogenic pollution is determined by the highest quartile of CO. The CO ~ 120 ppbv threshold during ARCTAS-B is chosen based on the PDF of CO (section 3).
[d] The CH_3CN ~ 145 pptv for ARCTAS-A and ~320 pptv for ARCTAS-B thresholds are chosen for the optimal segregation between the biomass burning and anthropogenic pollutions based on the CO_2/CO, CH_4/CO, and C_2H_6/CO ratio (supplementary Figures S1 and S2).

Table 3a. Mean observed chemical composition of air masses sampled during ARCTAS-A[a].

	Background				**Anthropogenic Pollution**	**Biomass Burning**	**Stratosphere**	**STE**
	2337 min (58%)				699 min (17%)	168 min (4%)	357 min (9%)	163 min (4%)
	0-12km	0-3 km	3-6 km	6-12 km	0-10 km[b]	3-9 km[b]	6-12 km[b]	5-12 km[b]
CO (ppbv)	144±14	156±5	148±9	135±15	**172±14**	**220±42**	48±14	103±14
O_3 (ppbv)	62±15	48±7	62±9	70±15	57±13	**78±12**	**363±122**	**142±31**
HO_x (pptv)	3.5±1.9	3.4±2.0	3.6±2.1	3.6±1.8	3.2±1.5	**6.7±4.2**	1.1±0.4	2.1±0.9
NO_x (pptv)	25±65	30±85	20±10	30±20	65±630	50±40	**150±55**	75±35
PAN (pptv)	205±80	220±60	225±85	180±80	**345±145**	**910±475**	70±30	170±50
HNO_3(pptv)	30±75	30±35	25±20	35±105	25±30	40±40	**1470±575**	**290±185**
ANs (pptv)	NA	NA	NA	NA	NA	**NA**	NA	NA
NO_y (pptv)	410±165	420±135	425±160	390±165	**650±660**	**1725±955**	**2035±660**	**790±270**

[a] For each type of air mass we include the observed mean ± one standard deviation. Chemical species that are significantly enhanced (> mean + one standard deviation) with respect to background at the corresponding altitude are highlighted in bold.
[b] The altitude span of individual air masses.

Table 3b. Same as Table 2a but for ARCTAS-B.

	Background				**Anthropogenic Pollution**	**Biomass Burning**	**Stratosphere**	**STE**	**Convection/ Lightning**
	1404 min (43%)				1207 min (39%)	325 min (10%)	32 min (1%)	142 min (4%)	61 min (2%)
	0-12km	0-3 km	3-6 km	6-12 km	0-12 km	0-10 km	10-12 km	6-12 km	6-12 km
CO (ppbv)	103±11	103±10	104±10	102±12	**153±39**	**426±280**	30±6	91±16	**149±29**
O_3 (ppbv)	57±20	34±6	60±15	69±20	58±19	48±17	**448±48**	**162±50**	78±10
HO_x (pptv)	9.1±5.1	9.8±6.5	10.3±5.0	7.1±2.9	11.8±7.8	**16.9±9.8**	1.2±0.3	4.4±1.8	5.0±2.9
NO_x (pptv)	25±30	35±45	20±20	30±25	**90±350**	**660±1520**	**385±50**	**110±60**	**625±375**
PAN (pptv)	210±100	105±55	230±80	245±95	**355±155**	**970±675**	70±50	320±45	**420±60**
HNO_3(pptv)	70±80	90±105	80±85	40±45	90±100	70±70	**1740±330**	**500±345**	25±20
ANs (pptv)	20±50	40±70	15±30	10±40	55±90	**205±260**	NA	45±65	**105±80**
NO_y (pptv)	315±165	245±200	310±140	365±145	**585±445**	**2055±2200**	**2210±260**	**955±350**	**1115±390**

Figure captions.

Figure 1. Flight tracks (black solid lines) of the NASA DC-8 aircraft for (a) ARCTAS-A and (b) ARCTAS-B. For this study, we only use measurements obtained north of 50°N. The color symbols indicate the location of various air masses sampled during ARCTAS. Tracks not marked with color symbols indicate background atmosphere.

Figure 2. Comparison of model CO with observations. Panel (a) shows the vertical profile of observed CO (red, error bars indicate the standard deviation of concentrations) and simulated CO (black line) during ARCTAS-A. Stacked influences from individual sources are also shown (green for NH biomass burning, blue for NH anthropogenic emissions, and gray for all other sources). Panel (b) shows the scatter plot of model CO vs. the observations during ARCTAS-A. The black solid line is the regression slope. Panels (c) and (d) are the same as (a) and (b) but for ARCTAS-B.

Figure 3. The probability distribution function (PDF) of observed CO (red line) and GEOS-5 CO (black line) along DC-8 flight tracks for ARCTAS-A. The mean PDF of model CO for April 2008 between 50°-90°N and 130°-180°W is shown in blue shading. For easy comparison with observations, we also include the corrected model CO distribution by shifting +25 ppbv to the right to account for the model low bias (black line-filled shading).

Figure 4. Same as figure 3 but for ARCTAS-B and the corrected model PDF is shifted +15 ppbv, instead of +25 ppbv, to the right to account for seasonal difference in model bias.

Figure 5. Probability distribution functions for the C_2H_2/CO ratio for (a) ARCTAS-A and (b) ARCTAS-B. We also plot the C_2H_2/CO ratio vs. CO (insets) to show the strong correlation between the two ($r = 0.81$ for ARCTAS-A and $r = 0.69$ for ARCTAS-B). Measurements associated with ODE events during spring (gray dots) and those associated with very fresh biomass burning plumes during summer (green dots) are excluded from the calculation of correlation coefficients for a better demonstration of the linear dependent relationship between CO and the C_2H_2/CO ratio in mean atmospheric condition.

Figure 6. Vertical profiles of CO and the C_2H_2/CO ratio during ARCTAS-A (panels a and b) and ARCTAS-B (panels c and b). Black lines show the mean background CO and C_2H_2/CO ratio at 1-km altitude bins, with gray shading indicating one standard deviation. We use colored symbols to show the individual air masses: stratosphere (purple), STE (lilac), anthropogenic pollution (blue), biomass burning (green), and convection/lightning (yellow). The solid color lines indicate the vertical mean profiles of individual air masses.

Figure 7. Top panels: Scatter plots of NO_x, PAN, HNO_3, and NO_y vs. CO during ARCTAS-A. Bottom panels: Similar to Figure 6, but the 1-km binned verticle profiles of NO_x, PAN, HNO_3, and NO_y during ARCTAS-A. The background air is shown in black and the individual air masses are shown in color: stratosphere (purple), STE (lilac), anthropogenic pollution (blue) and biomass burning (green).

Figure 8. Same as Figure 7 but for ARCTAS-B. Note part of the x-axis in the top panels for CO between 400-1000 ppbv is condensed in length for better visualization of the air mass characteristics.

Figure 9. Panels (a) and (c): The dependence of the instantaneous $NP(O_3)$ on NO_x for low (blue symbols) and high (red symbols) HO_x levels during ARCTAS. Panels (b) and (d): The dependence of the instantaneous $NP(O_3)$ on HO_x for low (blue symbols) and high (red symbols) NO_x levels. The instantaneous $NP(O_3)$ are calculated by the NASA Langley box model (Olson et al., 2004) constrained by chemical and physical parameters measured by the DC-8 aircraft. We separate data into low NO_x (HO_x) and high NO_x (HO_x) population using the mean conditions of the corresponding season, NO_x~40 pptv and HO_x~4 pptv in spring and NO_x~40 pptv and HO_x~10 pptv in summer. The low NO_x(HO_x) regime is highlighted in aqua shading on each panel.

Figure 10. Panel (a): Scatter plot of O_3 vs. CO during ARCTAS-A. Panel (b): Vertical profiles of O_3 during ARCTAS-A. Panel (b): Vertical profiles of instantaneous $NP(O_3)$ during ARCTAS-A. Similar to figure 7, the background air is shown in black and the individual air masses are highlighted in color: stratosphere (purple), STE (lilac), anthropogenic pollution (blue), biomass burning (green), and convection/lightning (yellow) Panels (d-f) are the same as (a-c) but for ARCTAS-B.

Figure 11. Vertical profiles of (a) NO_x, (b) O_3, and (c) instantaneous $NP(O_3)$ between 70°N-90°N during ARCTAS-B. Similar to figure 10, the background air is shown in black with individual air masses highlighted in color: stratosphere (purple), STE (lilac), anthropogenic pollution (blue), biomass burning (green).

Figure 1. Flight tracks (black solid lines) of the NASA DC-8 aircraft for (a) ARCTAS-A and (b) ARCTAS-B. For this study, we only use measurements obtained north of 50°N. The color symbols indicate the location of various air masses sampled during ARCTAS. Tracks not marked with color symbols indicate background atmosphere.

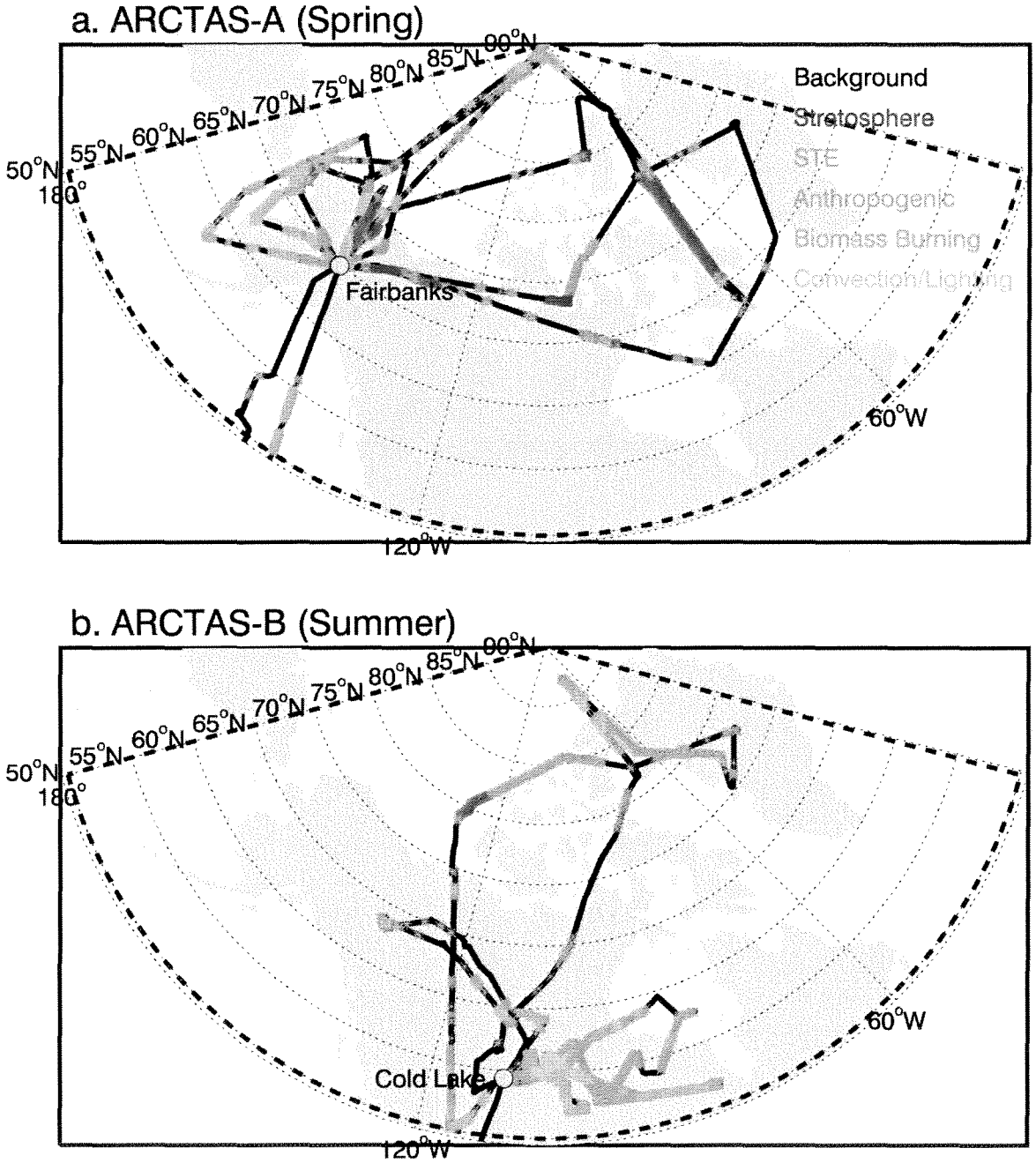

Figure 2. Comparison of model CO with observations. Panel (a) shows the vertical profile of observed CO (red, error bars indicate the standard deviation of concentrations) and simulated CO (black line) during ARCTAS-A. Stacked influences from individual sources are also shown (green for NH biomass burning, blue for NH anthropogenic emissions, and gray for all other sources). Panel (b) shows the scatter plot of model CO vs. the observations during ARCTAS-A. The black solid line is the regression slope. Panels (c) and (d) are the same as (a) and (b) but for ARCTAS-B.

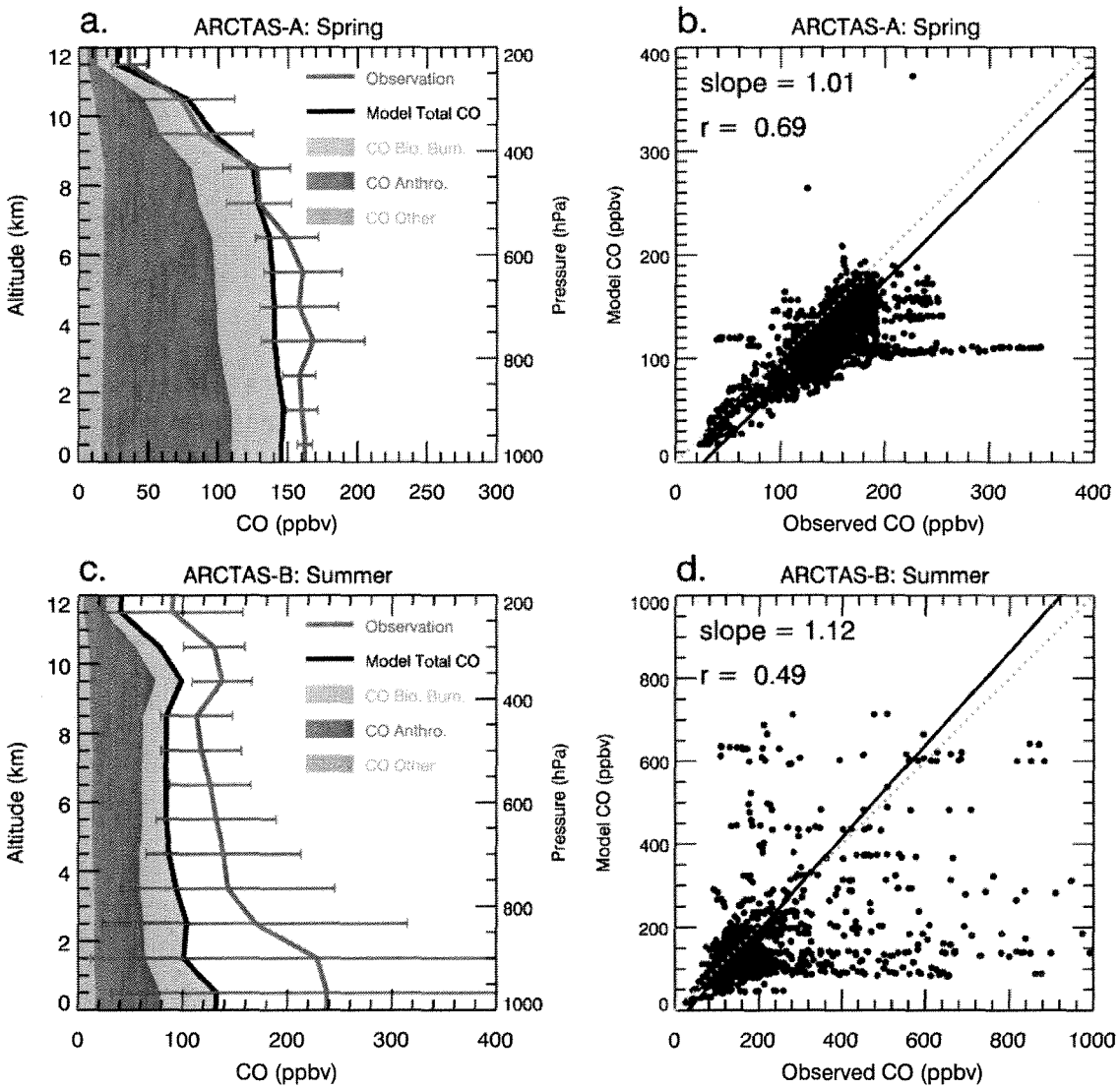

Figure 3. The probability distribution function (PDF) of observed CO (red line) and GEOS-5 CO (black line) along DC-8 flight tracks for ARCTAS-A. The mean PDF of model CO for April 2008 between 50°-90°N and 130°-180°W is shown in blue shading. For easy comparison with observations, we also include the corrected model CO distribution by shifting +25 ppbv to the right to account for the model low bias (black line-filled shading).

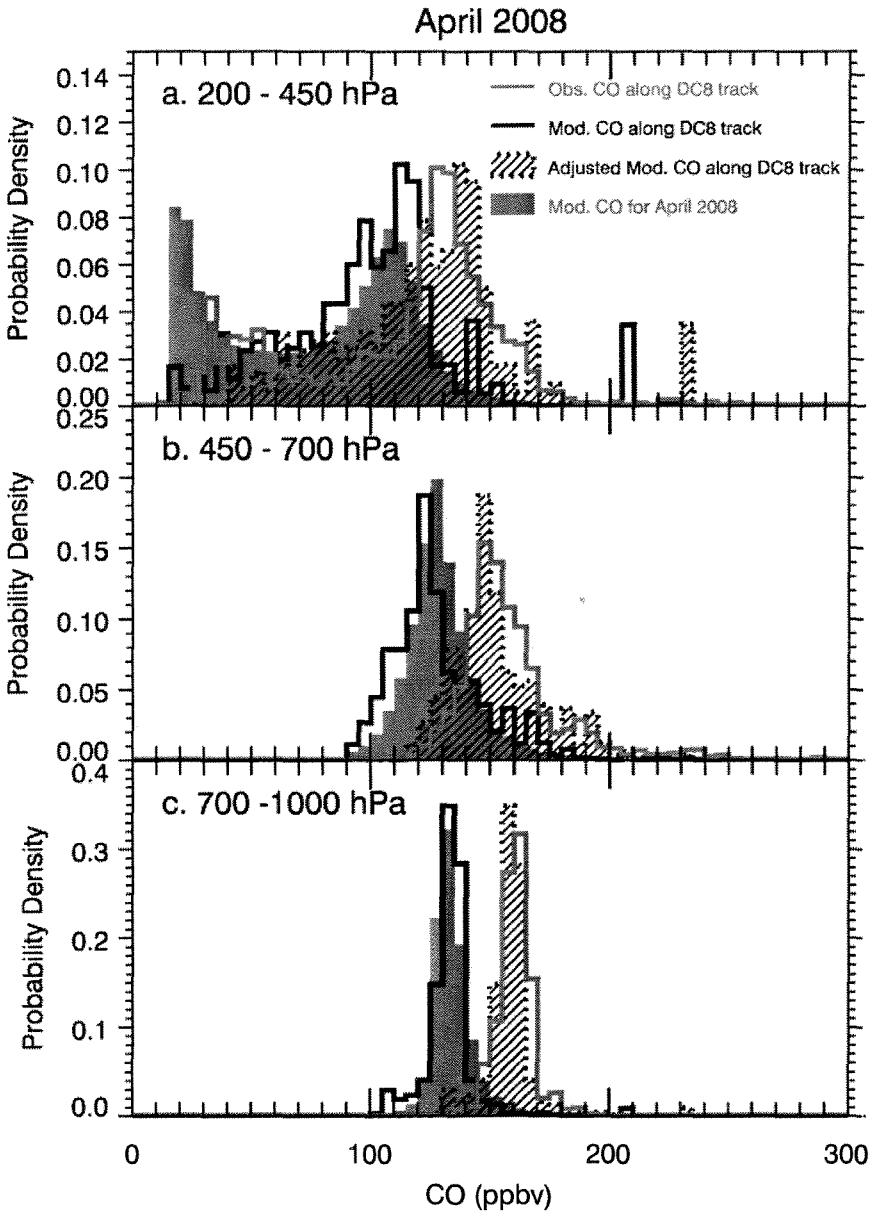

Figure 4. Same as figure 3 but for ARCTAS-B and the corrected model PDF is shifted +15 ppbv, instead of +25 ppbv, to the right to account for seasonal difference in model bias.

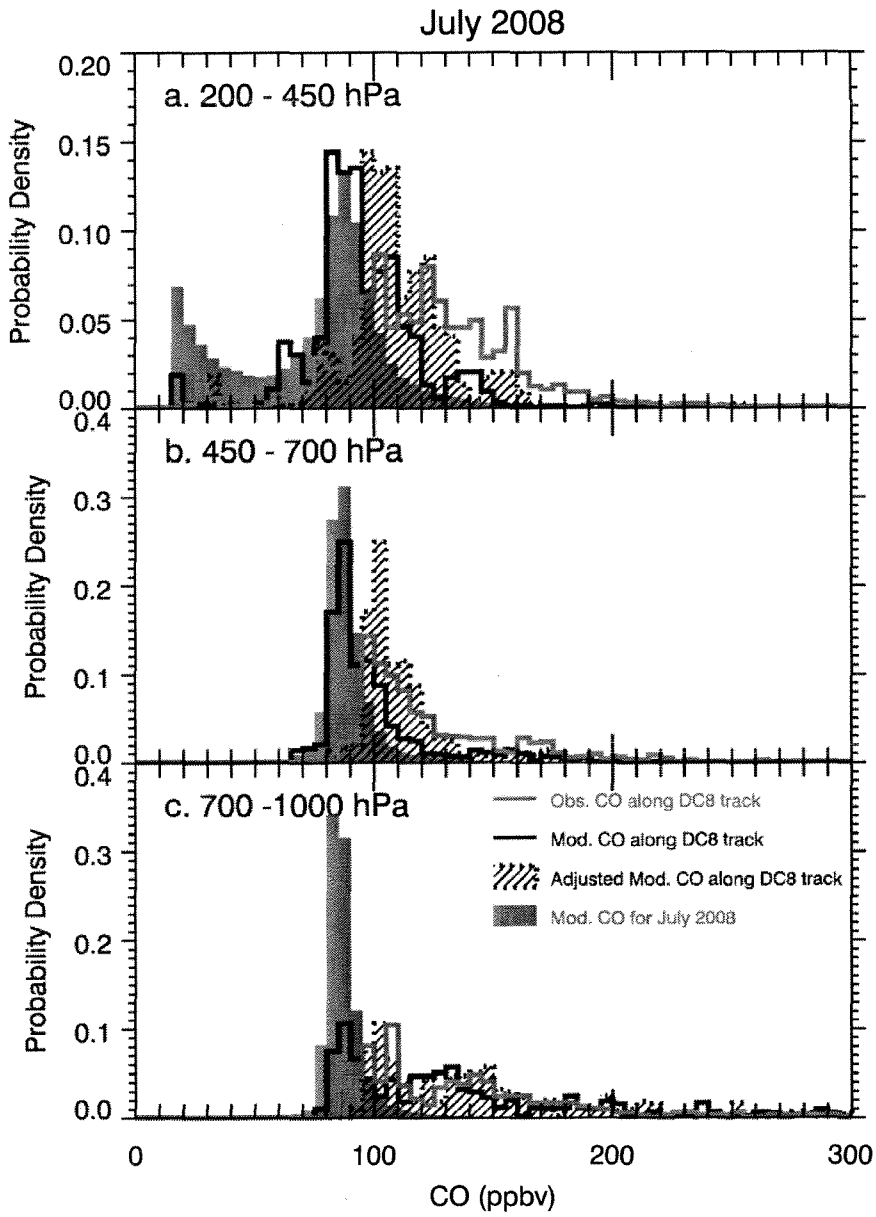

Figure 5. Probability distribution functions for the C_2H_2/CO ratio for (a) ARCTAS-A and (b) ARCTAS-B. We also plot the C_2H_2/CO ratio vs. CO (insets) to show the strong correlation between the two (r = 0.81 for ARCTAS-A and r = 0.69 for ARCTAS-B). Measurements associated with ODE events during spring (gray dots) and those associated with very fresh biomass burning plumes during summer (green dots) are excluded from the calculation of correlation coefficients for a better demonstration of the linear dependent relationship between CO and the C_2H_2/CO ratio in mean atmospheric condition.

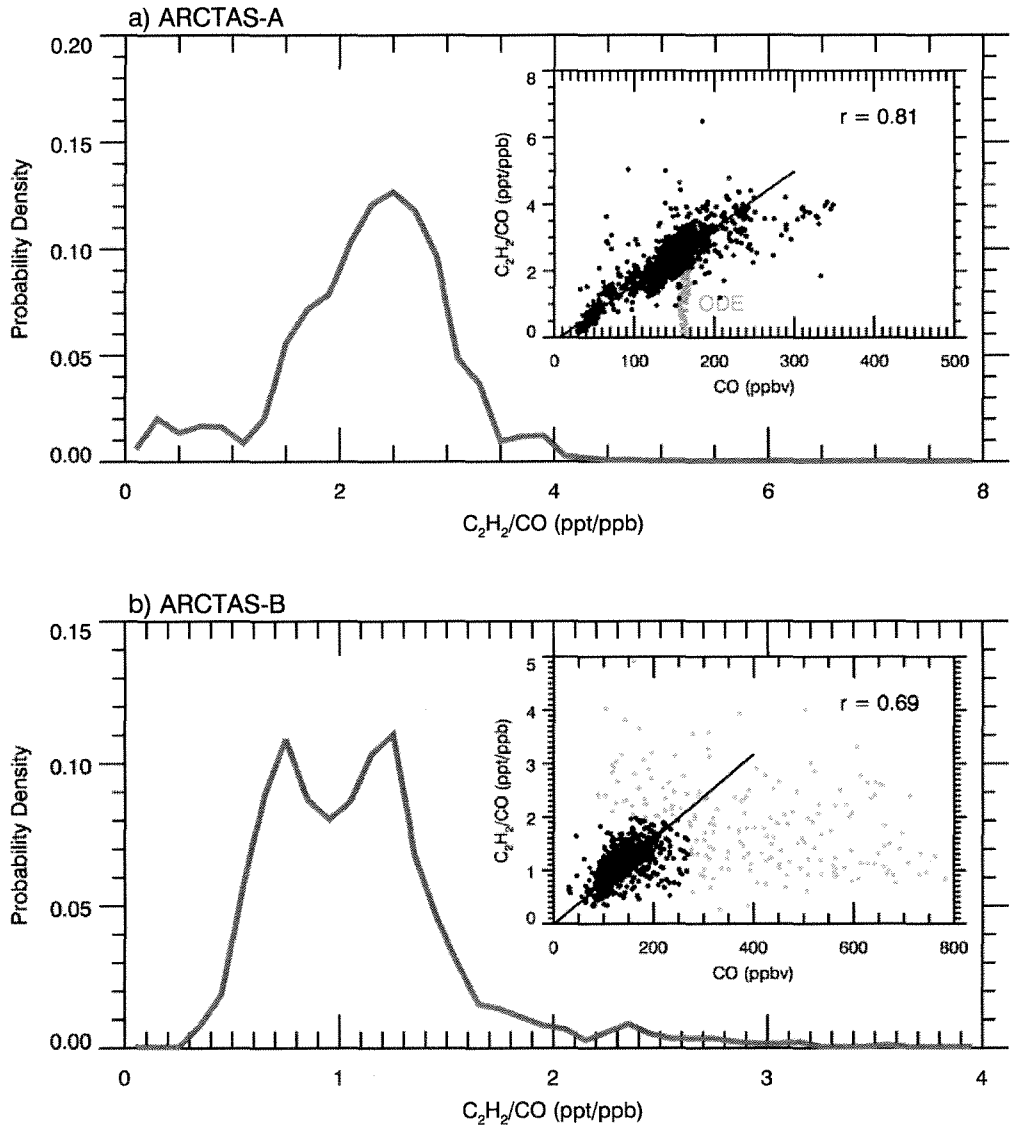

Figure 6. Vertical profiles of CO and the C_2H_2/CO ratio during ARCTAS-A (panels a and b) and ARCTAS-B (panels c and b). Black lines show the mean background CO and C_2H_2/CO ratio at 1-km altitude bins, with gray shading indicating one standard deviation. We use colored symbols to show the individual air masses: stratosphere (purple), STE (lilac), anthropogenic pollution (blue), biomass burning (green), and convection/lightning (yellow). The solid color lines indicate the vertical mean profiles of individual air masses.

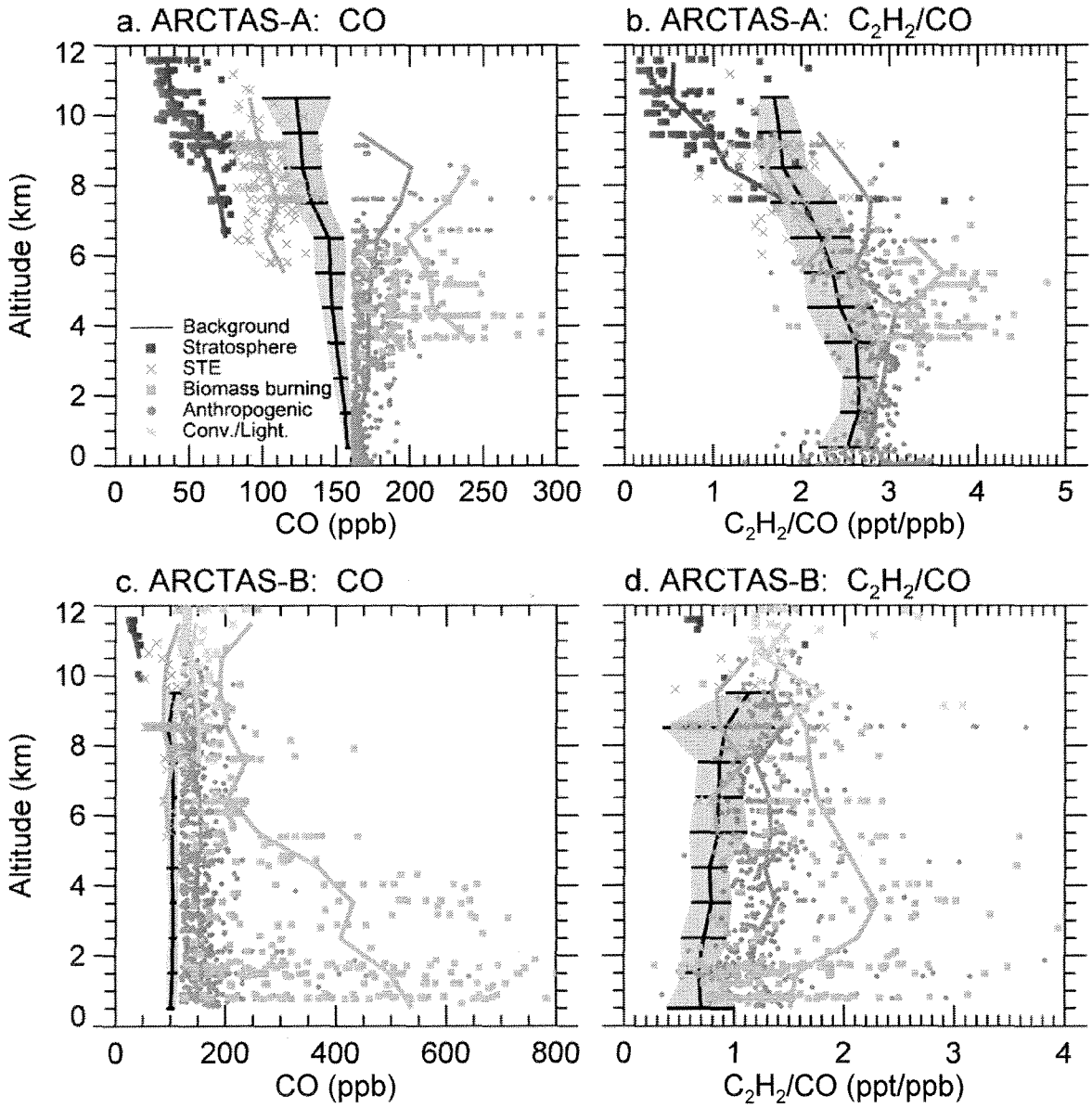

Figure 7. Top panels: Scatter plots of NO_x, PAN, HNO_3, and NO_y vs. CO during ARCTAS-A. Bottom panels: Similar to Figure 6, but the 1-km binned verticle profiles of NO_x, PAN, HNO_3, and NO_y during ARCTAS-A. The background air is shown in black and the individual air masses are shown in color: stratosphere (purple), STE (lilac), anthropogenic pollution (blue) and biomass burning (green).

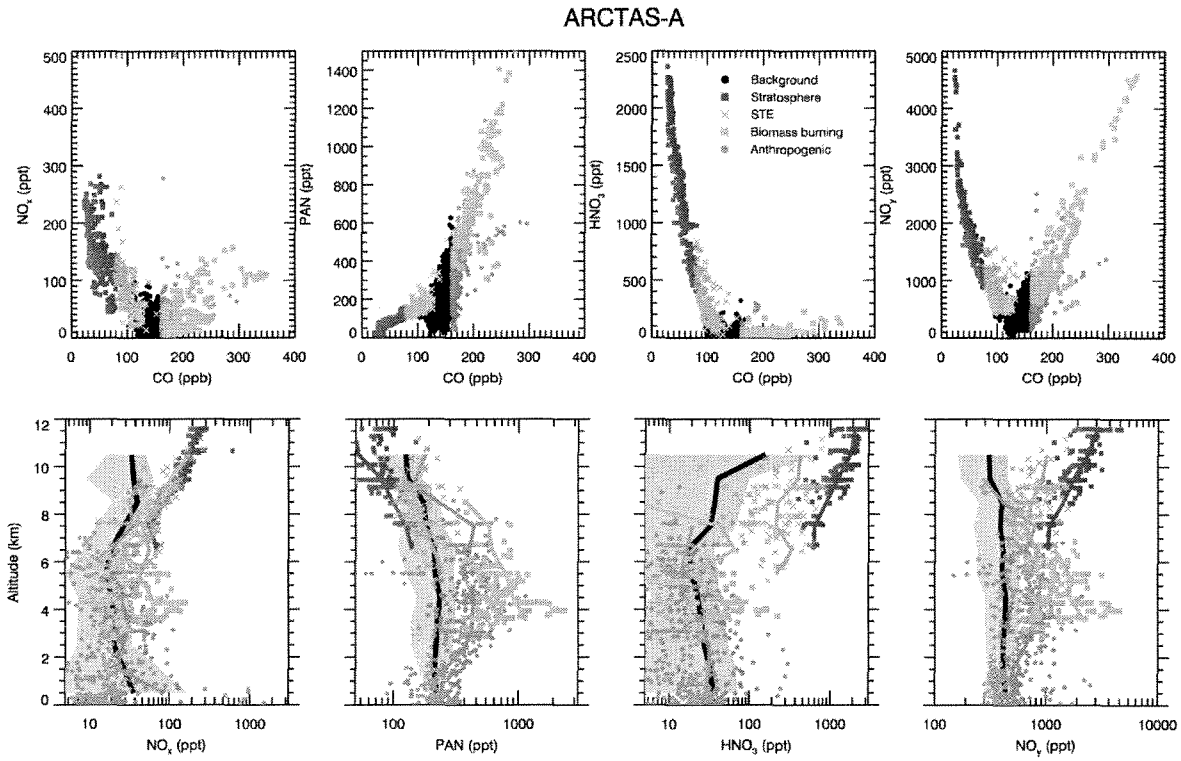

Figure 8. Same as Figure 7 but for ARCTAS-B. Note part of the x-axis in the top panels for CO between 400-1000 ppbv is condensed in length for better visualization of the air mass characteristics.

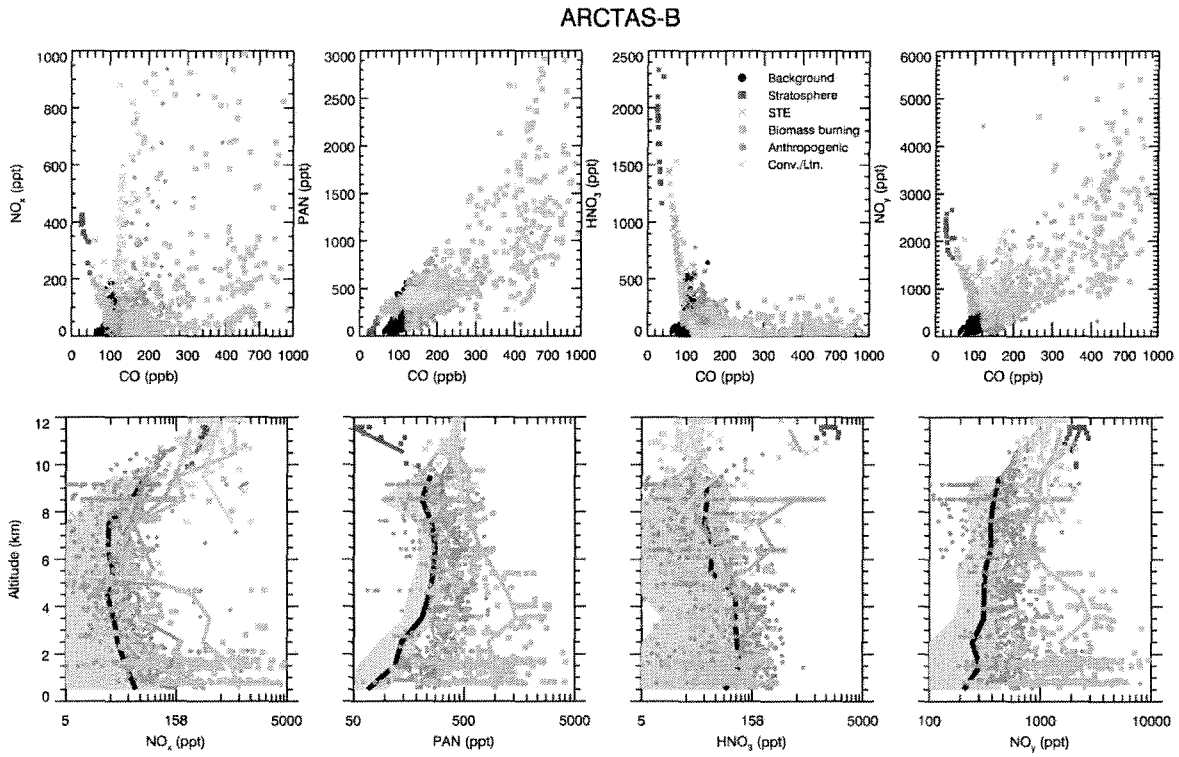

Figure 9. Panels (a) and (c): The dependence of the instantaneous $NP(O_3)$ on NO_x for low (blue symbols) and high (red symbols) HO_x levels during ARCTAS. Panels (b) and (d): The dependence of the instantaneous $NP(O_3)$ on HO_x for low (blue symbols) and high (red symbols) NO_x levels. The instantaneous $NP(O_3)$ are calculated by the NASA Langley box model (Olson et al., 2004) constrained by chemical and physical parameters measured by the DC-8 aircraft. We separate data into low NO_x (HO_x) and high NO_x (HO_x) population using the mean conditions of the corresponding season, NO_x~40 pptv and HO_x~4 pptv in spring and NO_x~40 pptv and HO_x~10 pptv in summer. The low NO_x(HO_x) regime is highlighted in aqua shading on each panel.

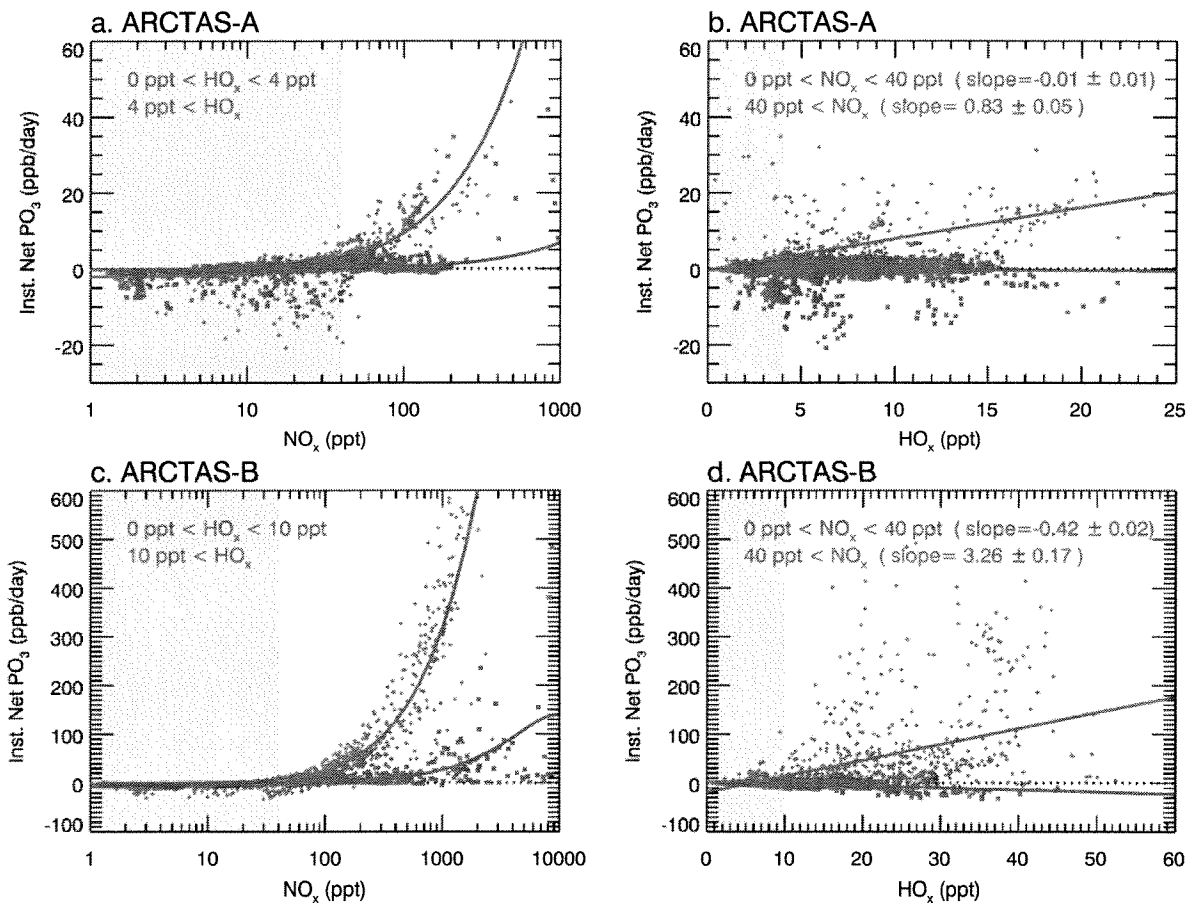

Figure 10. Panel (a): Scatter plot of O_3 vs. CO during ARCTAS-A. Panel (b): Vertical profiles of O_3 during ARCTAS-A. Panel (b): Vertical profiles of instantaneous $NP(O_3)$ during ARCTAS-A. Similar to figure 7, the background air is shown in black and the individual air masses are highlighted in color: stratosphere (purple), STE (lilac), anthropogenic pollution (blue), biomass burning (green), and convection/lightning (yellow) Panels (d-f) are the same as (a-c) but for ARCTAS-B.

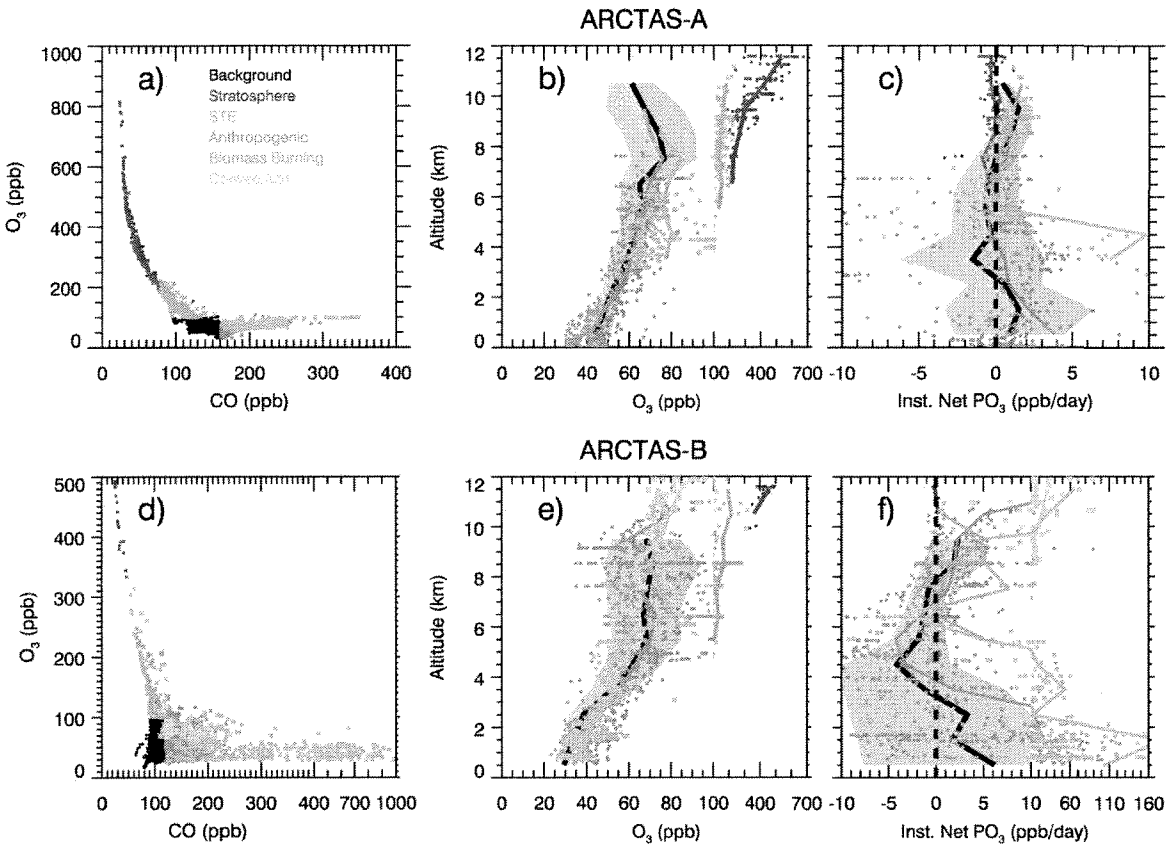

Figure 11. Vertical profiles of (a) NO_x, (b) O_3, and (c) instantaneous $NP(O_3)$ between 70°N-90°N during ARCTAS-B. Similar to figure 10, the background air is shown in black with individual air masses highlighted in color: stratosphere (purple), STE (lilac), anthropogenic pollution (blue), biomass burning (green).